Ministry of Higher Education and Scientific Research
University of Baghdad
Institute of Laser for Postgraduate Studies

Relative Humidity Sensor Based on No Core Multimode Interferometer Enhancement using Al_2O_3-PVA Composite Films

A Thesis Submitted to the Institute of Laser for Postgraduate Studies, University of Baghdad in Partial Fulfillment of the Requirements for the Degree of Master of Science in Laser / Electronics and Communication Engineering

By
Hiba Yassin Al-shafai

B.Sc. Laser and optoelectronic Engineering – 2015

Supervisor
Asst. Prof. Dr. Hanan J. Taher

2020 AD **1441AH**

بِسْمِ اللهِ الرَّحْمنِ الرَّحِيمِ

﴿وَلَمَّا بَلَغَ أَشُدَّهُ وَاسْتَوَى آتَيْنَاهُ حُكْمًا وَعِلْمًا وَكَذَلِكَ نَجْزِي الْمُحْسِنِينَ ﴾

﴿ And when he had attained his maturity, We gave him wisdom and knowledge: and thus do We reward those who do good.﴾

صدق الله العلي العظيم

سورة القصص الآية (14)

Certification

I certify that this thesis was prepared under my supervision at the Institute of Laser for Postgraduate Studies, University of Baghdad, as a partial fulfillment of requirements for the degree of "Master of Science in Laser/ Electronics and Communication Engineering".

Signature:

Name: **Dr. Hanan J. Taher**

Title: **Asst. professor**

Address: Institute of Laser for Postgraduate studies,

University of Baghdad.

Date: / / 2020

(Supervisor)

In view of the available recommendation, I forward this thesis for debate by Examining Committee.

Signature:

Name: **Asst. prof. Dr. Hanan Jaafar Taher**

Title: Head of the Scientific Committee.

Address: Institute of Laser for Postgraduate studies, University of Baghdad.

Date: / / 2020

Examination Committee Certification

We certify that we have read this thesis " **Relative Humidity Sensor Based on No Core Multimode Interferometer Enhancement using Al_2O_3-PVA Composite Films**" and as Examination Committee, we examined the student in its content and in our opinion, it is adequate with standards as a thesis for a degree of Master in science in Laser /Electronics and Communication Engineering.

Signature:

Name: Asst. prof. Dr. Zainab Fadhil Mahdi

Title: Assistant Professor.

Address: Institute of Laser for Postgraduate studies, University of Baghdad.

Date: / / 2020

(Chairman)

Signature:

Name: Asst. prof. Dr. Mohamed K. Dhahir

Title: Assistant Professor.

Address: Institute of Laser for Postgraduate studies

University of Baghdad.

Date: / / 2020

(Member)

Signature:

Name: Asst. prof. Dr. Shaymaa Riyadh Tahhan

Title: Assistant Professor.

Address: University of AL-Nahrain

Date: / / 2020

(Member)

Signature:

Name: Asst. prof. Dr. Hanan J.Taher

Title: Assistant Professor.

Address: Institute of Laser for Postgraduate studies,University of Baghdad.

Date: / / 2020

(Supervisor)

Approval by the Deanship of Institute of Laser for Postgradgate Studies, University of Baghdad.

Signature:

Name: Asst. prof. Dr. Hussain A.Jawad

Title: Assistant Professor.

Address: Dean of Institute of Laser for Postgraduate studies, University of Baghdad.

Date: / / 2020

الاهداء.....

إلهي لا يطيب الليل إلا بشكرك ولا يطيب النهار إلى بطاعتك.. ولا تطيب اللحظات إلا بذكرك .. ولا تطيب الآخرة إلا بعفوك.. ولا تطيب الجنة إلا برؤيتك

الله جل جلاله

الى منارة العلم والامام المصطفي إلى الأمي الذي علم المعلمين إلى سيد الخلق إلى رسولنا الكريم

سيدنا محمد صلى الله عليه واله وسلم

إلى الينبوع الذي لا يمل العطاء إلى من حاكت سعادتي بخيوط منسوجة من قلبها إلى كل من في الوجود بعد الله ورسوله

إليك امي اهدي هذه الرسالة

إليك أماه.. قطرة في بحرك العظيم.. حباً وطاعة وبرا

الى من علمني الصبر ومعاناة الصعاب لاصل الى ما انا فيه

الى ابي

إلى من حبهم يجري في عروقي ويلهج بذكراهم فؤادي

إلى أخواتي وأخواني

إليك حبيبي أحضرت شيئاً من الثمر
فأنت سقائي بعد الله.. وأنت المطر

اليك زوجي العزيز..

إلى من زرعوا التفاؤل في دربي وقدموا لي المساعدات والتسهيلات والأفكار

والمعلومات، فلهم مني كل الشكر الى صديقاتي وأخص منهم: نور عدنان، سارة جمال،

غفران عبد القادر

إلى من لم أعرفهم ..... ولن يعرفوني

إلى من أتمنى أن أذكرهم..... إذ ذكروني

ACKNOWLEDGEMENTS

I would like to thank my supervisor assist. Prof. **Dr. Hanan J.Taher** for her guidance, kind advice, continuous follow, encouragement and help through the period of research and during writing of this thesis.

My deep and sincere thanks to **Eng. Saif Akeel Mohammed** for his valuable advice and motivation.

I would like to introduce a great thank to **Dr. Mohamed K. Dhahir** for his continuous help through this work.

I would like to thank assist. Prof **Dr. Zainab Fadhil** for helping me

I would like to introduce a great thank **Dr. Ali Salman**, **MSC.Ansam Majid** for their continuous valuable comments on the experimental part.

Kind thanks are going to all the staff of the Institute for their effort during this research work.

I would like to express my thanks to "**my friends**", for their never ending moral support.

Finally, I would like to express my greatest thanks to "**my family**", for their sincere support and reliance.

ABSTRACT

Optical fiber relative humidity (RH) sensor based on etched no-core fiber (NCF) multi-mode interferometer (MMI) is widely used in the sensing region. The sensor structure was constructed by fusion splicing a segment of no-core fiber (NCF) between two single-mode fibers (SMFs) to sense the changes of the external RH. Various tuned diameters of NCF from 125 μm to (100, 75 and 50) μm, with a fixed length of 20 mm of the NCF were obtained by chemical etching with hydrofluoric acid (HF). The sensor was constructed by fusion-splicing (60, 40, 20) mm length of NCF with optimum diameter 50μm between two segments of SMFs to study the affect of the length on the sensor sensitivity. The optimum performance of the proposed sensor in sensing the variation in relative humidity was the NCF with diameter 50μm and 20mm length for the sitting sensor structure. The experimental results exposed that sensitivity enhanced more than twice was obtained at the proposed optimum NCF coated with aluminum oxide nanoparticles (Al_2O_3 NP_s) embedded in polyvinyl alcohol (PVA). The maximum sensitivity of 0.587 nm/%RH was obtained in the RH range of 30% to 100% with 6s response time. The proposed sensor can establish a promising source for RH monitoring.

TABLE OF CONTENTS

LIST OF TABLES

LIST OF FIGURES

LIST OF ABBREVIATION

RH	Relative Humidity
SMF	single-mode fiber
NCF	no-core fiber
SMS	single-mode-multimode-single-mode
MMF	multi-mode fiber
POFs	plastic optical fibers
PVA	Polyvinyl alcohol

Al_2O_3	Aluminum oxide
NA	Numerical aperture
OFSs	Optical fiber sensors
MMI	Multimode interference
PC	polarization controller
FBG	fiber Bragg grating
MZIs	Mach-Zehnder interferometer sensor
OC	Optical coupler
LPGs	long period gratings
RI	Refractive index
SNCS	single mode-no-core-single mode fiber
OSA	Optical spectrum analyzer
B.B.S	Broadband source
TEC	thermoelectric cooler
PVC	Polyvinyl chloride
HF	hydrofluoric
SEM	Scanning electron microscopy
GQDs	Graphene quantum dots
CuO	Copper Oxide
LiCl	Lithium chloride

LIST OF SYMBOLS

n_c	Refractive index of the core	
n_{cl}	Refractive index of the cladding	
n_1	Refractive index of the glass	
n_2	Refractive index of the air	
θ_c	Critical angle	Degree,radian

D_{NCF}	The diameter of NCF	μm
L_{NCF}	Length of the NCF	mm
L_{π}	Beat length	
m	Self-imaging number	
n_{NCF}	the effective refractive index of NCF	
λ_0	interference wavelength	nm
λ	Wavelength	nm
P_{v}	Partial pressure of the water vapor	Pascal
$\mathrm{P_s}$	Saturation water vapor pressure	Pascal

Chapter One

Introduction and Basic Concept

1.1 Introduction and Motivation

Monitoring of relative humidity (RH) has undergone considerable focus in recent years owing to their numerous applications such as chemical, medical and environmental applications [1-3]. Fiber sensors of interference class are extensively used due to their several advantages compared to their electronic counterparts like compactness, simple fabrication; immunity to electromagnetic interference and their ability to broadcast a vast amount of data over a long fiber span [4]. However, humidity-induced changes in the refractive index are usually ultra-small, leading to significant difficulties in directly measuring relative humidity (RH). Therefore, many kinds of materials combined with various fiber structures have been investigated and exploited to enhance the sensitivity to RH. These fiber-optic humidity sensors include different hydrophilic coatings have been applied on the fiber surface like polyvinyl alcohol [5-6], agarose [7], graphene oxide [8-9] and metal oxide film [10-11], In these materials, swelling occurs after absorption of water and a refractive index modification to the surrounding medium takes place by the change in RH. The operating principles of these sensors rely on the interaction of the evanescent wave of light traveling through the fiber with the surrounding.

Based on the previous reports, the design of an optical fiber humidity sensor is basically divided into two steps. The first step is the fabrication of an optical fiber sensing platform, and the second is the deposition of a coating material. The single-mode–no-core–single-mode fiber (SNCS) structure is a good platform for the fabrication of simple and cost-effective optical fiber sensors [7][86]. As RI is a function of RH, so the increase of RI of the surrounding environment will lead to an increase in the sensitivity of SNCS sensor where the surrounding air works as a cladding of NCF [7]. In addition,

decreasing the diameter of the no-core fiber (NCF) in such structures is considered to be as an efficient method to improve the sensitivity of the sensing system [95].

To maximize the evanescent field, the tapering of the NCF cladding can be achieved by heat pulling or chemical (hydrofluoric acid) etching [22]. Tapering and coating the active sensing segments (i.e. NCF) with nanoparticles (NPs) can promote the sensor's sensitivity [22, 83, 86]. The nanostructures coating on the tapered NCF portion induce changes of the optical fiber properties in response to an external medium. The RH can be monitored through the RI changes of the coating material.

Up to date, nanostructured thin films have been applied to diverse optical fiber structures to fabricate new sensors to detect RH such as plastic optical fibers (POFs) [12-13], side-polished fibers [13-14], photonic crystal fibers [15], tapered fibers [16] and single-mode-multimode-single-mode (SMS) [17]. Based on the previously published reports, the process of demonstration such optical fiber RH sensor includes the fabrication of an optical fiber sensing platform, and then deposition of coating material on the surface or end face of the optical fiber.

On the other hand polymers like polyvinyl alcohol (PVA) coated fiber have been recently reported as an enhanced humidity sensitive material in constructing RH sensors, due to their unique advantages like good sensitivity, low cost and a good capability for film-forming with a refractive index comparable to that of silica glass[6, 78].

Several techniques are available at present to form composite thin films [16,31]. Among several techniques, the dip coating method was considered as one of the most prominent methods, because of the advantages of low cost with ease in preparation of thin films [86].

Al_2O_3 NPs as a type of transition metal oxide with ceramic structure seem a promising humidity-sensitive coating due to its attractive properties such as hardness, high melting point and hydrophilic property [18]. Moreover, Al_2O_3 has been used as an adsorbent, desiccating agent, and catalyst material which makes it interested to use as a coating in optical fiber humidity sensors (OFHS) [19].

1.2 Optical fibers

The optical fiber is a dielectric waveguide that is employed to keep and direct the "light" [20]. Usually this optical fiber is made from silica glass or plastic. Principle work of optical fiber based on total internal reflection. The core is a thin center of the fiber where the light travels and is generally made of glass with refractive index (n_1) is slightly higher than that of the cladding (n_2) [21]. The difference between core and cladding refractive indices gives the ability to guide the light [22] Conventional optical fibers can be classified depending on their structure or waveguide modes the single mode fiber or multimode fiber. They also multimode fibers may be classified depending on the how refraction index changed between core and cladding step index fiber or graded index fiber. The core diameters of the single mode fibers and multimode fibers are different, where, the single mode has a small core diameter of about (8-10 μm), while the multimode has large core diameters about (50 or 60 μm) or may be larger [23, 24].

1.2.1 Classification of Optical Fibers

Optical fiber can be classified into two main types, single mode fiber and multi-mode fiber as shown in figure (1-1)[25].

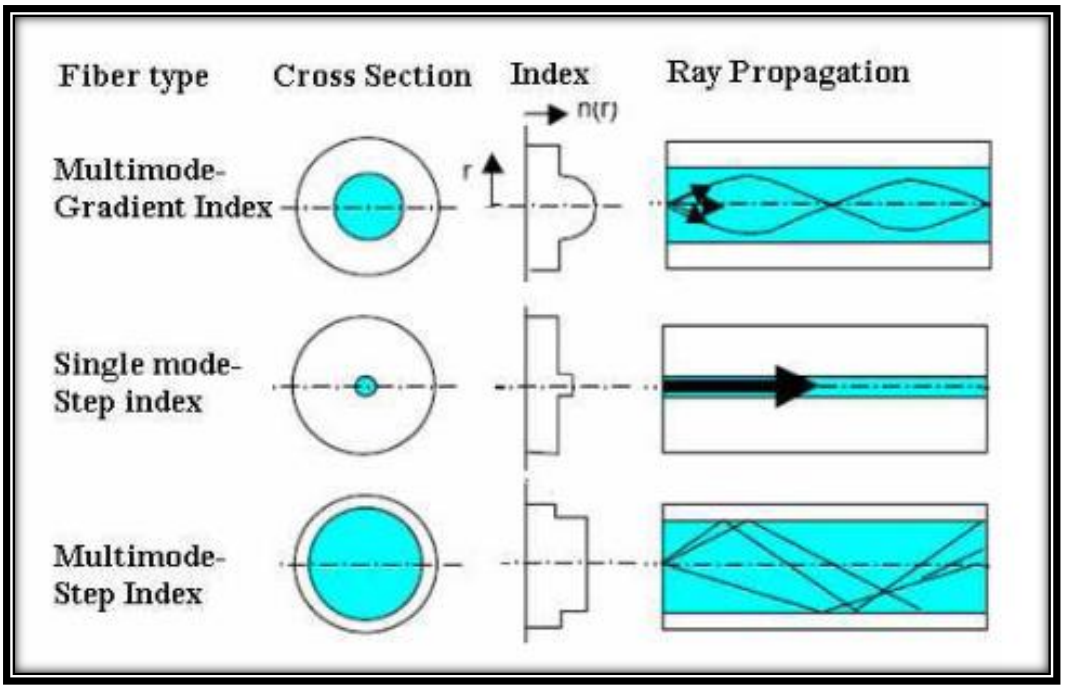

Figure (1-1): The types of optical fibers [25].

1.2.1.1 Single mode fiber (SMF):

Optical fibers that permit to a single mode of transmit light to propagate through it. Single mode fiber mainly associated with a core small in diameter (8-10 μm) [26], The core refractive index can be indicated as n_1 which is greater than cladding refractive index n_2. The small diameter of the core allows it to transmit one mode of light. No dispersion, no degradation of the signal travelling through the fiber, Low attenuation due to the number of waves that propagate along the core of fiber which gives the ability to the signal to propagate for long distances and faster [27].

1.2.1.2 Multi-mode fiber (MMF):

Optical fibers permit to multi modes of transmitting light to propagate through it. MMF has a large core diameter of about (50-60μm) [26]. Also, the relative refractive index is larger than SMF. High attenuation and dispersion is obtained due to the number of modes that propagate along with the core thus the signal quality will be not appropriate for protracted space communication [27]. There are two categories of multi-mode fibers depending based on refractive index profile [27]

i. **Step index multimode fiber:** optical fiber that have a larger diameter of the core (about 50 -200 μm). In this type the path of the light propagation is zig-zag in form. The refractive index of the core is (n_c) and that of cladding is (n_{cl}), the refractive index of the core remains constant (n_c) and suddenly changes to (n_{cl}) inside the cladding. the total internal reflection takes place due to change in the refractive index at the core cladding interface , as the light rays move from the core to cladding (denser to rarer medium)[27].

ii. **Graded-index multimode fiber:** optical fiber that has a diameter of the core is about (50) μm. In this type the path of light is helical in form. The refractive index of the core (n_c) is maximum at the center of the core and decreased gradually to a minimum value (n_{cl}) at the core-cladding interface. The light rays moving down the axis advance more slowly than those near the cladding because of their difference in their refractive indices. But almost all the rays reach the exit at the same time due to the helical path. So, there is no dispersion [27].

iii. No-core fiber (NCF)

NC fiber considered as a special type of multimode fiber with uniform RI. The loss of cladding, the core of the NC fiber is directly in contact with the external environment creating a multimode waveguide NCF has only a core with 125µm diameter usually made from fused silica which is the same as conventional fibers outer diameter [28].

NC fiber fabricated by different companies with various operation temperatures (-65±300 Cº), different diameters ranged (125-480) µm, also a wide range of operating wavelengths (400-2400) nm for several applications. The surrounding medium of NCF which is lower than NC fiber refractive index acts as cladding based on the total internal reflection [29].

Figure (1.2) shows a comparison between the SMF and the NC fiber schematic.

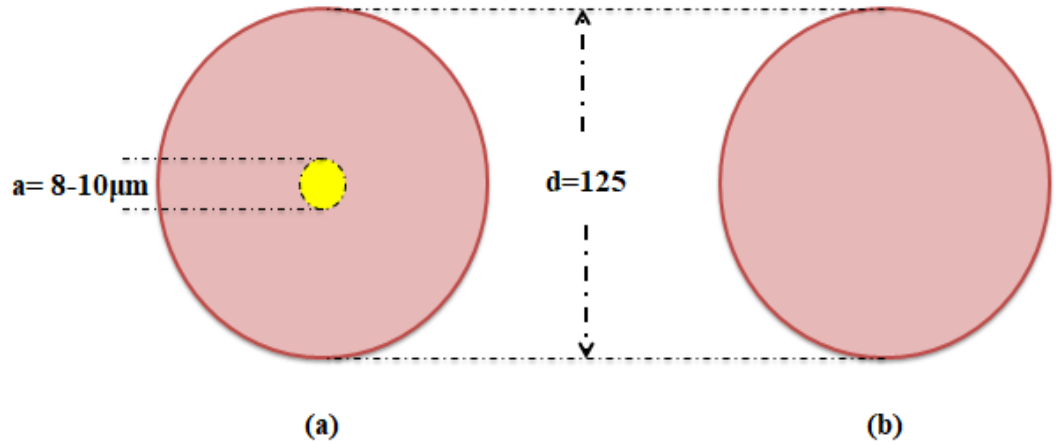

Figure 1.2 Comparison between the single mode fiber and the NC fiber schematically [28].

1.3 Propagation of Light within an Optical Fiber

In order for the couple ray of light into the optical fiber can be explained by the ray theory, it is substantial to observance account of the refractive index of the medium. The refractive index of the medium is a value calculated from the ratio of the velocity of light in a vacuum to the velocity of light in the medium of greater density. The light ray is traveling more fast from optically minimal dense medium than through optically that is more denser, where the refractive index profile describes this influence[32]. When a ray of light incident on the boundary between two different isotropic like glass and air, the refraction phenomena was happened. For example, when the light ray incident on one end of optical fiber at a certain angle to its axis, it travels in zig-zag form and the total internal reflection happen at core-cladding interface and injected to the another end of the fiber[26]. TIR phenomenon happens when light ray travels from a medium of refractive index n_1 and is at an angle φ_1, approaches the other side of lower refractive index n_2 at an angle φ_2 greater than incident angle φ_1 ,where calculated with respect to the normal. The refraction φ_2 and the incidence angles φ_1 are related to each other and to the refractive indices, where given by Snell's law refraction [33]:

$$n_1 \sin \varphi_1 = n_2 \sin \varphi_2 \qquad (1.1)$$

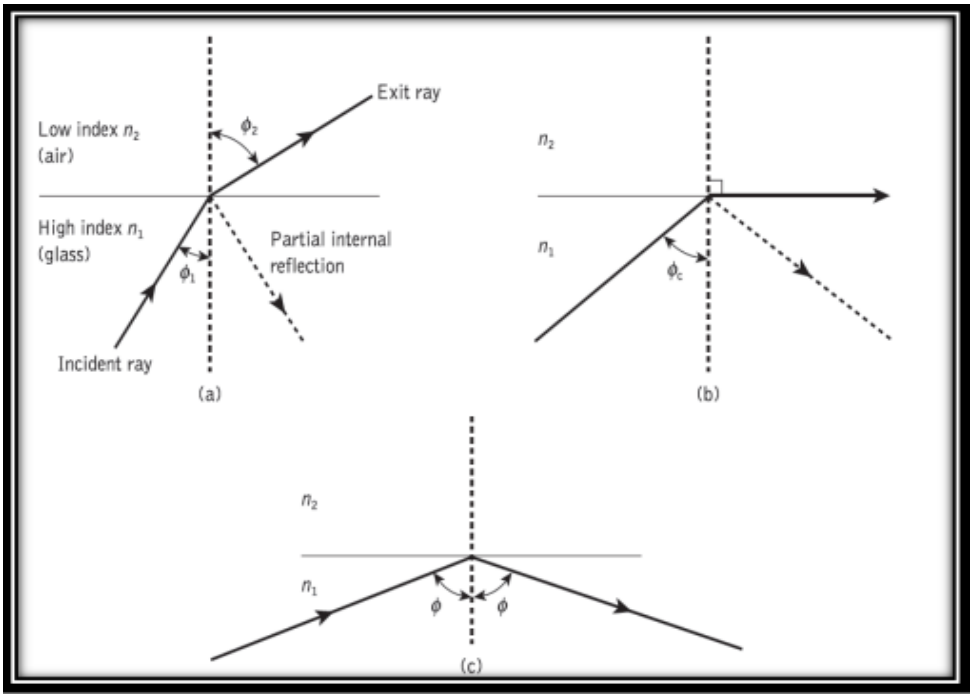

Figure 1.3 Light confinement in optical fiber. (a) The refraction (b) The refraction case explaining the critical angle φ_c, and (c) The TIR where φ greater than φ_c [32].

From figure 1.3 (a) when a light incident at the medium with refractive index n_1 to another medium with lower refractive index n_2, the refraction depends on the refracted angle which is always greater than the incidence angle. The critical angle φ_c is the incidence angle when the angle of refraction ray is 90° as shown in figure1.3 (b) and could be given by [32]:

$$\varphi c = \sin^{-1}\frac{n_2}{n_1} \qquad (1.2)$$

If the light incident at an angle greater than the critical angle φ_c, then all the light beam will be reflected into one medium as illustrated in figure 1.3 (c) TIR occurs where $n_2<n_1$ [32]. Figure (1.4) illustrate the light ray enters the optical fiber and reflected at the first core-cladding interface at the angle θ. This light ray enters the fiber core at an angle of incidence θ_{in} which is called the acceptance angle for which the ray undergoes TIR at the core-cladding interface and propagates along the fiber [33].

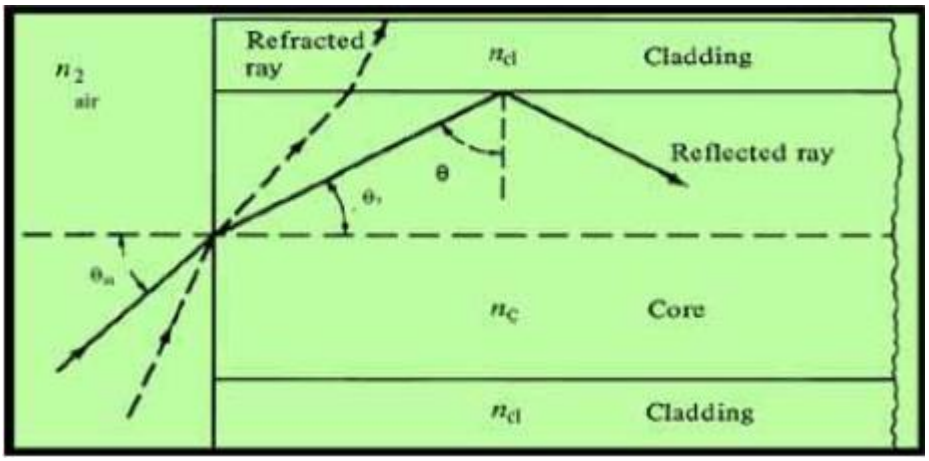

Figure (1.4): the transmission of light through an optical fiber [33].

The sine of the acceptance angle of the fiber represented by the numerical aperture (NA) which for light ray launched a fiber from the air (n_2=1) is given by [34] [35]:

$$NA = (n_c^2 - n_{cl}^2)^{1/2} \quad (1.3)$$

1.4 Optical fiber sensor (OFS)

Optical fiber sensor has been fabricated to measurement several parameters which used in various applications, like as pressure, refractive index, temperature, rotation, acceleration, vibration, magnetic fields, strain and humidity [36-45]. Optical fiber sensors have gained a lot of interest due to their potential applications in civil, military, medicine, and industry applications [46-50]. Optical fibers are typically employed for monitoring the changing in environmental and has many advantages such as quality improvement, small size, light weight, robustness, low cost of some types, flexibility, electromagnetic immunity and high sensitivity While some of its disadvantages are very expensive, carefully handling and unfamiliarity to the end user. But its appealing advantages show the possibility of the fiber optic [51].

1.4.1 Types of Fiber Sensors

In general, optical fiber sensors can be divided into four classes based on changes in optical parameters such as polarization, intensity, wavelength, and phase sensor [52].

Wavelength modulation based optical fiber sensor was used in early optical sensor development due to its low cost, simplicity, and reliability [53]. The wavelength of light source passed through a sensor head from a light varies by the measured. The wavelength of modulated light can be measured by a light receiving component and transformed into an electrical signal. The electrical signal change is proportional to the change of the measured. Many sensors, like humidity and refractive index sensors have been implemented based on this modulation technique [54, 55].

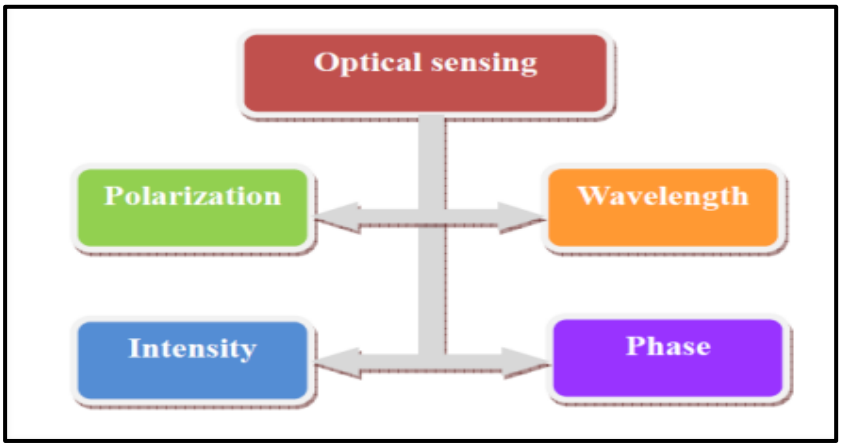

Figure (1.5): Categories of optical sensors [53].

Optical fiber sensors (OFSs) are classified into two basic types extrinsic (hybrid) fiber sensors or intrinsic (all-fiber) fiber sensors [56]. Figure (1.6a) illustrates the schematic diagram of an extrinsic optic-fiber sensor; the optical fiber is used as an appliance for transporting the light to and from an external sensing system where the process of the sensing occurs [56].

In an intrinsic (all- fiber sensors), the fiber is used as a transmitter and at the same time the fiber itself works as the sensing as shown in figure (1.6b). To increase the sensitivity of this type of optical sensor, the slight modification of optical fiber occurs due to the environmental effects [56- 58].

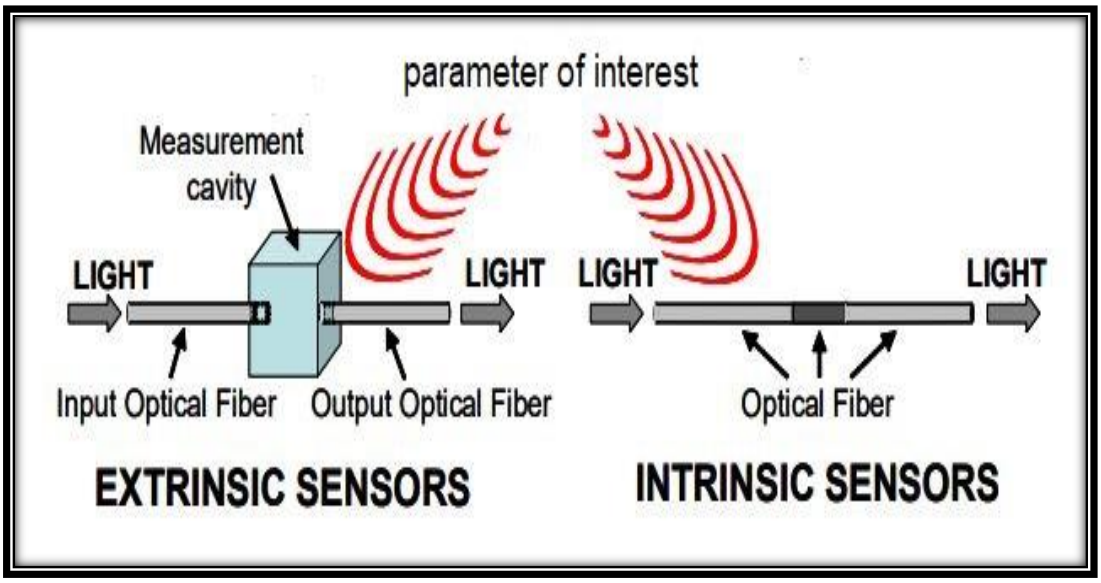

(a) **(b)**

Figure (1.6): a schematic diagram of: (a) Extrinsic fiber sensor and, (b) intrinsic fiber sensor[56]

1.5 Multi-mode interference (MMI) optical fiber sensors:-

Multi-mode interference (MMI) Optical Fiber sensor within a segment of multi-mode fiber (MMF) provides a useful basis for emerging a variety of fiber optic devices and sensors, filters, RI sensors, temperature sensors, RH sensors [59]. These sensors have properties of operating over moderate distance with good optical power, cost effectiveness, and high sensitivity [60]. In order to use multi-mode interference devices in sensing systems, the physical variable capable of either modify the multi-mode fiber parameters or interact with the modes of propagating.

MMI sensor usually fabricated by a splicing piece of MMF between two single mode fibers [61]. The length and diameter of MMF plays a significant role in the formation of propagation modes. The environmental changes affected the effective refractive index and resulted in variation in central wavelength which is the key parameter in MMI sensor detection. The incident field from SMF higher order modes will excited together with the fundamental mode of the NC fiber. These modes interfere along the NC fiber length and are subject to the multimode interference effect then these modes recombined in the other end of SMF at the second splicing point [61]. Therefore, that the length and diameter of NC fiber plays important role in the formation of these multimode interference phenomena.

1.6 Applications of Optical fiber sensors:

Optical fiber sensors are utilized in many fields especially [94]:

1- Observation of the physical health of structures in real time.

2- Used to measure the physical properties of humidity, temperature, strain, velocity, and displacement [30,31].

3- Application to the gas and oil industry, pressure sensing, temperature sensing.

4- Tunnels: Multipoint optical extensometers, convergence monitoring, and joints monitoring damage detection.

5- Heritage structures: old-new interaction, post-seismic damage evaluation, Displacement monitoring, restoration monitoring.

6- Dams: distributed temperature monitoring, spatial displacement measurement, Foundation monitoring, joint expansion.

1.7 Optical Interferometer:

In the sensing region, optical fiber interferometers give elegant performance in high sensitivity, wide dynamic range, and high accuracy. Also, the optical fiber technology gives a large number of liberty degrees and some features like mechanical stability, small size and absence of moving parts for the construction of interferometers. A modal interferometer needs large components like beam splitters, lenses and coupler needed to fabricate an optical fiber interferometer [58, 64].

A lot of information about spectral and temporal state of the signal given by interferometers that make possible to detect any variation with bandwidth, wavelength , intensity, phase and so on with the ambient variation. In the sensing region, optical fiber interferometers give elegant performance in high sensitivity, wide dynamic range, and high accuracy [39].

Optical fiber sensors based on interferometer utilize the interference happens between two beams with two different optical paths and the interference could happen in single fiber or into individual fibers. So that beam collecting and beam splitting components required [65]. Of course, one of the optical paths must be arranged with ease affected by external fluctuation. The best structure applied in the optical fiber interferometer is in-line structure, in this structure the two optical paths located in a single physical line. Several advantages like as easy alignment, high stability, and high coupling efficiency provided by in-line structure [66**]**.

1.7.1. Sagnac fiber interferometer

A sagnac interferometer contains a fiber optic loop which made by splicing a piece of long conventional SMF fiber to fiber coupler with two output port in which light is split into two beams and propagate in opposite different directions inside the same waveguide in a fiber loop as shown in Figure (1.7) [67]. A polarization controller (PC) used to adjust the polarization. The path of the lunched beam is modified resulting in a phase shift and a different interference pattern because of the effect of environmental parameters in the sensing region [74].

3 dB couplers used to split the input light and the two beams recombined in the same coupler. Birefringent fibers used in the sensing part to increase the polarization [67].

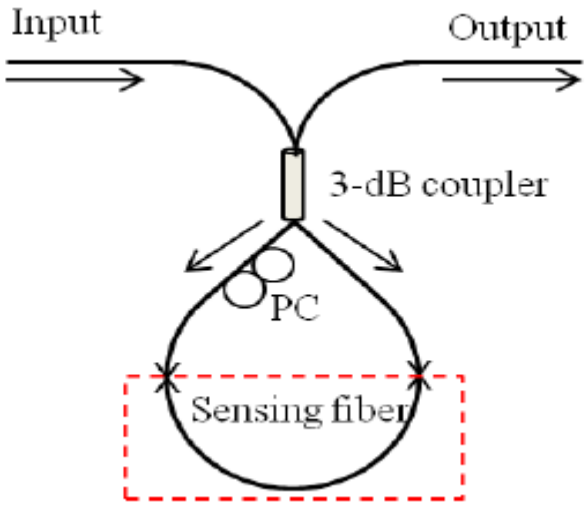

Figure (1.7):A sagnac fiber interferometer [67]

1.7.2 Fabry-Perot Interferometry Sensor

This type of optical interferometer which shown in figure (1.8) comprises two optical reflectors placed in parallel separated with a certain distance L between those reflectors [68]. It is also called an etalon [69]. Reflectors can be an interface of two dielectrics mirrors, or two fiber Bragg gratings, or two internal mirrors achieved by splicing of polished fibers, or by coating cleaved end of the optical fiber [70].

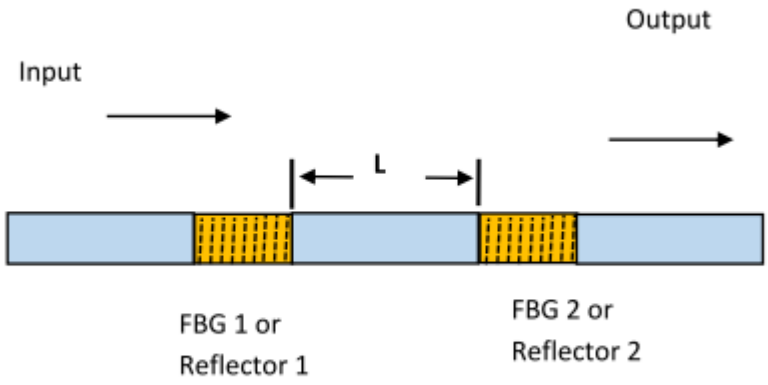

Figure (1.8): The Schematic diagram of FPIs [70].

1.7.3 Michelson fiber Interferometer

Michelson interferometers optical fiber sensors are similar to MZIs sensors, both of them contain two arms and the sensing depends on interference between these arms. The difference between them is that Michelson interferometers sensors have reflecting mirror at the end of each arm as shown in figure (1.9). The launched beam will split in to two different optical paths and reflect at the end of fiber by mirrors or other optical reflectors recombined by the optical coupler (OC) to create the interference pattern at the output end [71].

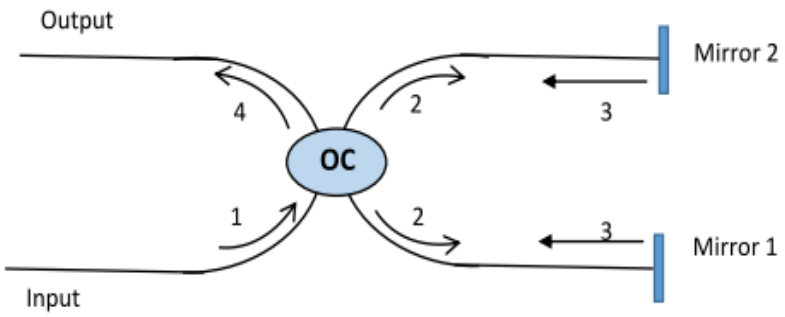

Figure 1.9 (a) Michelson interferometer Schematic diagram[72].

1.7.4 Mach-Zehnder interferometers Sensors

Mach-Zehnder interferometer sensors have found a wide range of sensing applications due to their flexibility and easy to fabricate. The MZI structure contains of two arms, the reference arm and sensing arm [64], the first fiber coupler is used to split the incident light into two arms as shown in figure(1.10). Another fiber coupler is used to recombine split light. The interference appears in the recombined light between the two MZI arms according to optical path difference, Therefore one of these arms will be maintained isolated from any external variation and the external variation exposed to the sensing arm such as humidity, temperature, refractive index, strain applied on sensing arm changes the optical path difference of MZL, and could be detected as variation in the interference signal [73].

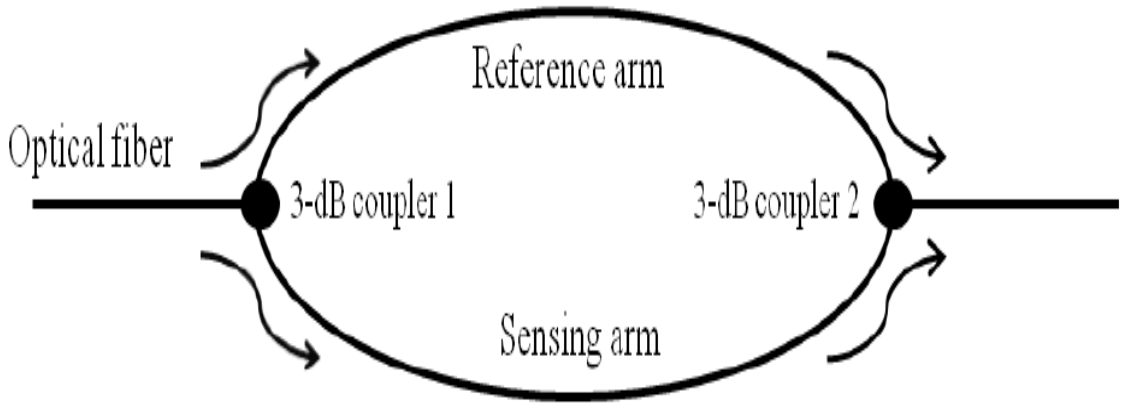

Figure (1.10): The schematic diagram of MZIs[67].

There are various kinds of in-line MZI sensors[67] such as interferometers built with tapered, singlemode-multimode-singlemode (SMS) MZI, interferometer based on long period gratings (LPGs) and interferometers fabricated developed with core mismatch and MZI with Micro-hole collapsing as shown in figure (1.11)

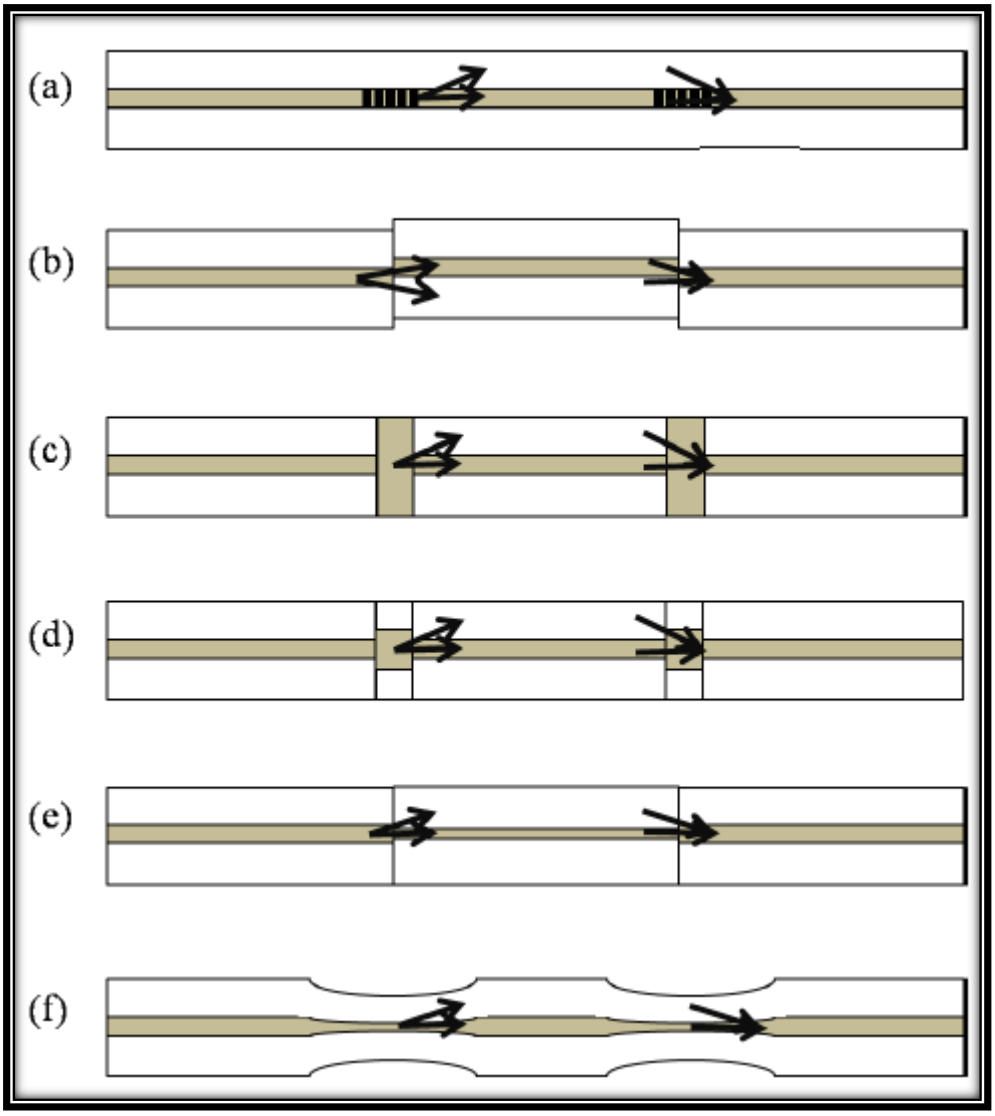

Figure (1.11); Schematic of different kinds of MZI (a) a pair of LPGs, (b) core mismatch, (c) PCF air-holes collapse region, (d) Multi-Mode fiber, (e) SMF small core, and (f) fiber tapered.[67]

1.8 Humidity sensing

Humidity refers to the ratio of the water vapor content in the atmosphere of air to the saturation value or other gases. It is a very important physical amount to be measured. So it has significant importance in a range of various areas from daily life as shown in figure (1.12) including the food industry,

chemical manufacturing, civil engineering, weather prediction, and meteorological services[70]. Relative humidity (RH) is the ratio of the partial pressure of water vapor show in the air at a particular temperature to the maximum vapor pressure of water at the same given temperature. The RH is determined as a percentage, using the expression (1.4) [70] [96]:

$$RH = \frac{P_V}{P_s} \times 100\% \qquad (1.4)$$

Where P_V the partial pressure of the water is vapor and P_s is the saturation water vapor pressure. RH is a relative measurement because it is a function of temperature.

The sensitivity of the sensor (S) is calculated , using the expression (1.5)

$$S = \left(\frac{\Delta\,\lambda}{\Delta\,RH}\right)$$

Where $\Delta\,\lambda\,is$ the change in wavelength and $\Delta\,RH$ is the change in a relative humidity.

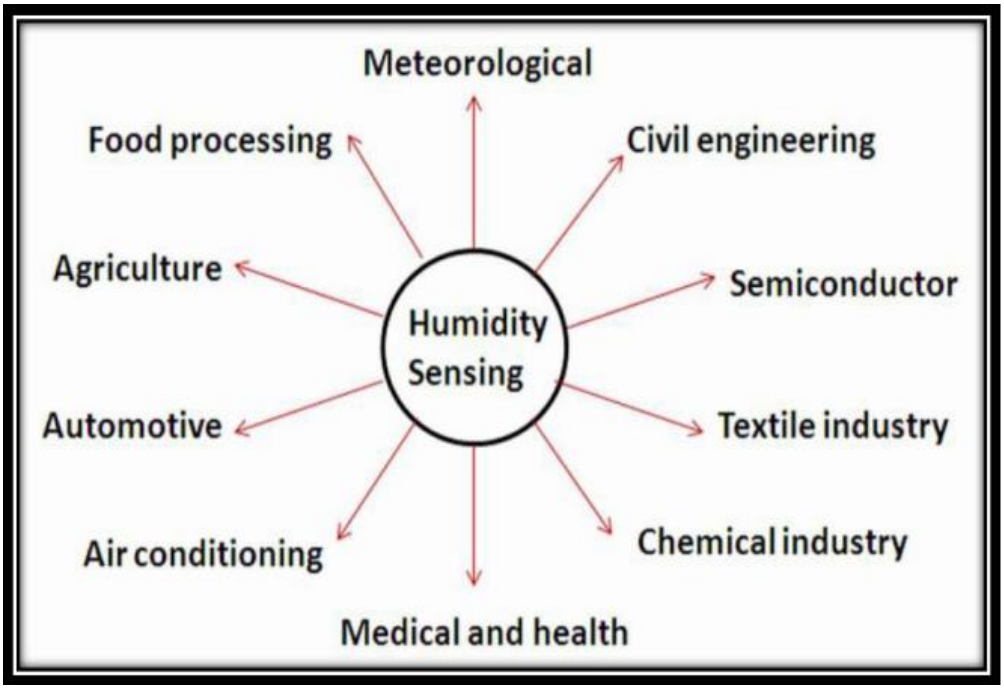

Fig (1.12): applications of humidity sensors in variety of areas [70].

1.9 Operating Principle of the RH Sensor based on SNCS

No core fiber (NCF) is used for a single-mode multimode single-mode (SMS) fabrication. To provide a good RH sensitivity to the device increase the evanescent waves by fiber etching and coating, when the incident light propagates from the input SMF to NCF, the higher-order modes will be exited [7]. During propagation along NCF part, they will experience interference which leads to a multimode interference (MMI). To have a self-image right at the output of the SMF, the performance of the proposed sensor is essentially related to the variation in the refractive index of the surrounding medium of NCF. By changing the relative humidity, the RI around NCF region would change which leads to shifting in output wavelength [71].

1.10 Literature survey

Various optical fiber humidity sensors such as multimode interference (MMI) have been demonstrated for different applications such as bacterial growth, food processing, weather monitoring and industrial operation. Because, they have the advantages of small size and weight, low cost, simple fabrication [3]. Number of research papers were used to build and study various relative humidity optical fiber sensor, some of previous works and contributions in the field of thesis interest have been introduced in table (1-1)

Table (1-1): Summary of the Published Works in OFHS

Year	***Author***	***Structure and illumination source and coating***	***Sensitivity***	***Ref.***
May 2011	Qiang Wu et al.	SMF-small core of SMF-single mode fiber structure (SMF-SCSMF-SMF) , Broad band source (1500-1600)nm coating with polyethylene oxide (PEO)	0.436 nm/%RH in humidity ranged from 40% to 95% RH	[76]
July 2011	Yu Zhao et al.	SMS, amplified spontaneous emission ASE (1520-1534)nm, PVA	0.18nm/RH in ranged 80% to 89%	[77]
April 2013	Jiali .An	SMS coating with PVA , (ASE) (1520-1580), ranging From 30% to 80% RH	0.09nm/%RH	[78]
August 2014	Jiali An et al.	SMS with two waist-enlarged tapers coating With PVA, in humidity ranged from 35%-85% RH	0.223 nm/RH	[79]
Octobr 2015	Chujia Huang	porous anodic alumina (PAA) coating on tip of SMF tip by using 1550 nm Super Luminescent Diode with range of RH from (20%–90%)RH	0.31nm/%RH	[80]

Year	***Author***	***Structure and illumination source and coating***	***Sensitivity***	***Ref.***
August 2017	Wei Xu	SNCS, broad band source (1500-1600)nm coated with Agarose	0.149nm/%RH	[81]
2017	Diego Lope. Torres	SMF-PFC-SMF, SnO 2 thin films on to PCF, A multi-LED light (HP83437A) source	0.96nm/%RH	[82]
2017	Haitao Yan	D-shaped fiber, PVA-Au coating , amplified spontaneous emission (ASE) source (1525 to 1610 nm)	5.4nm/%RH	[83]
February 2018	Y.Zho	Interferometer U-shaped microfiber(MF) coated with PVA, ranged from 30%RH to 95%RH, spontaneous emission source (ASE)	186.5 pm/%RH	[84]
December 2018	Y.Zho	Fabry–Perot RH sensor coating with polyimide(PI) on The end of MMF system, Tungsten Halogen Light Sources with Wavelength range (360–1050 nm)	0.164 nm/%RH	[85]
Oct – Dec 2018	Huda .A	SNCS fiber structure coating with CuO-PVA ,Broad band source (BBS),range from 30% to 100%	-0.581 nm/%RH	[86]

Year	***Author***	***Structure and illumination source and coating***	***Sensitivity***	***Ref.***
2019	Y.Zho	hollow core fiber coating with GQDs-PVA film ,Broadband(ASE),Range from 11.3–81.34%RH	0.11725 nm/%RH	[87]

1.10 Aim of the work:-

The motivation for this work is to fabricate a humidity sensors based on multimode interferometer using NCF, The specific objectives of the work are as follows:

1. Enhancement of the optical fiber humidity sensor utilizing a multimode no-core optical fiber with a metal oxide Al_2O_3/PVA coating layer

2. Study the influence of reduction of NC fiber diameter in the enhancement of the sensor sensitivity.

3. Study the influence of the change of NCF length on the sensitivity.

4. Study the effect of the Al_2O_3 NPs coating layer on the active segment of the sensor parameters.

Chapter Two

Experimental Setup and Procedures

2.1 Introduction

In this chapter, all parts of the system were explained. The experimental setup and work procedure for the fabrication of a humidity sensor based on SNCS fiber structure were illustrated. The sensors under investigation were based on Multimode Interferometer (MMI) based on a collapsing technique which was used in this work as a modal interferometer. SNCS fiber sensors was fabricated and constructed by cleaving and splicing different lengths of NCF (from Thorlabs) with conventional optical fiber (SMF-28).

Sensor sensitivity was enhancement by etching process which applied to NCF to tune its diameter or coated of the active segment of the sensor with a nanomaterial.

The schematic block diagram summarizes the experimental work as shown in figure (2.1).

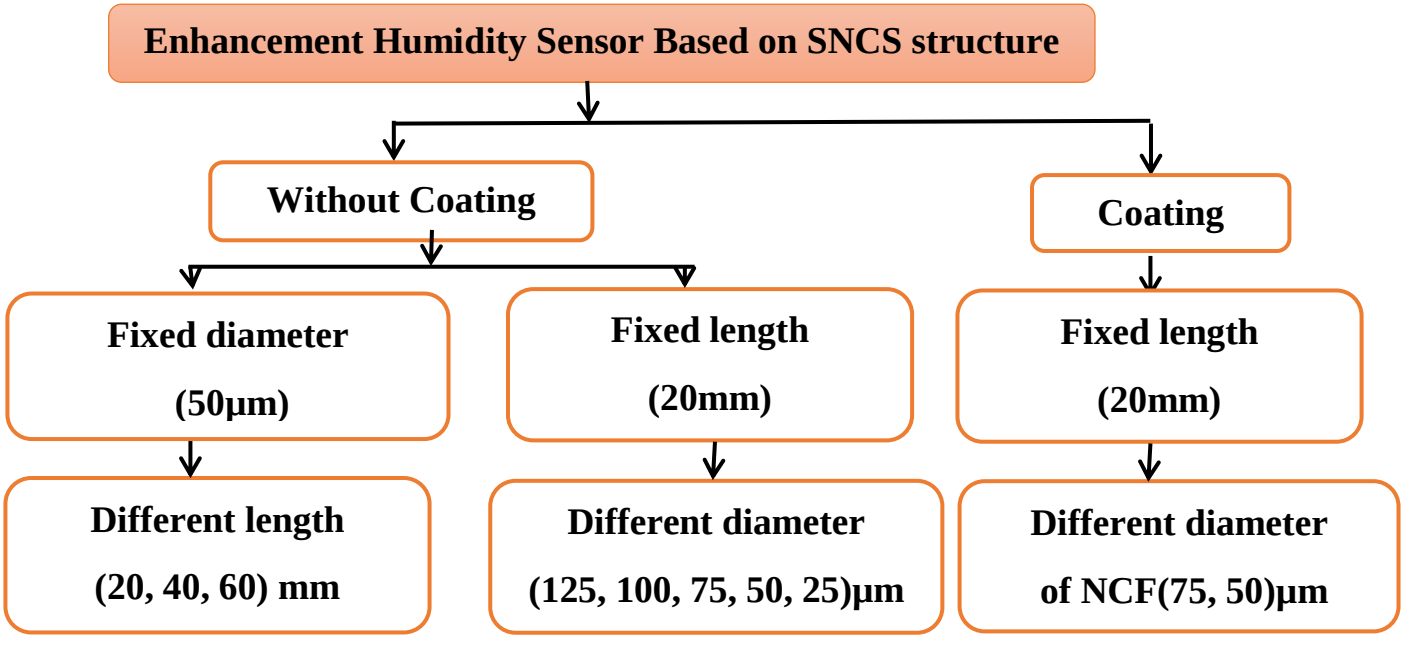

Figure (2.1) The schematic block diagram of experimental work

2.2 System Layout:-

The relative humidity sensor based on SNCS system layout is shown in figures (2.2) and (2.3).

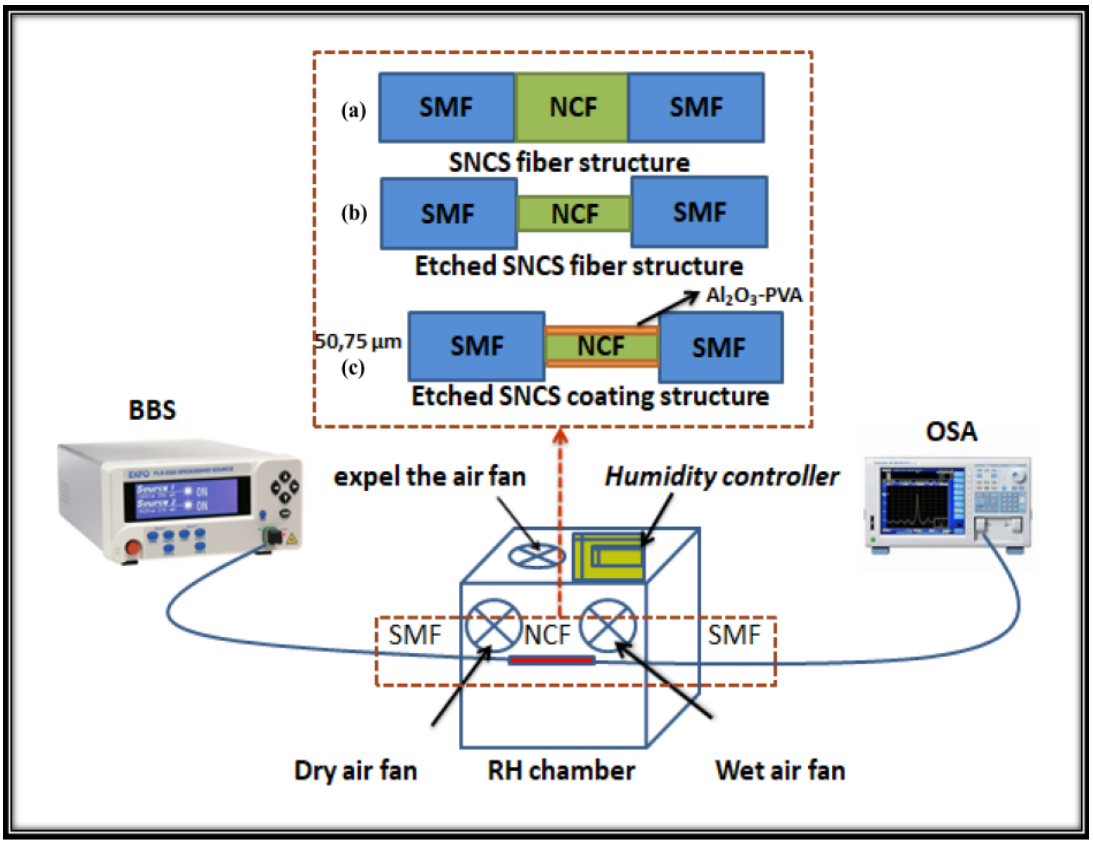

Figure (2.2) the experimental setup for measuring the RH based on SNCS fiber structure

(a)SNCS fiber structure (b) Etched SNCS fiber structure (c) Etched SNCS coating fiber structure

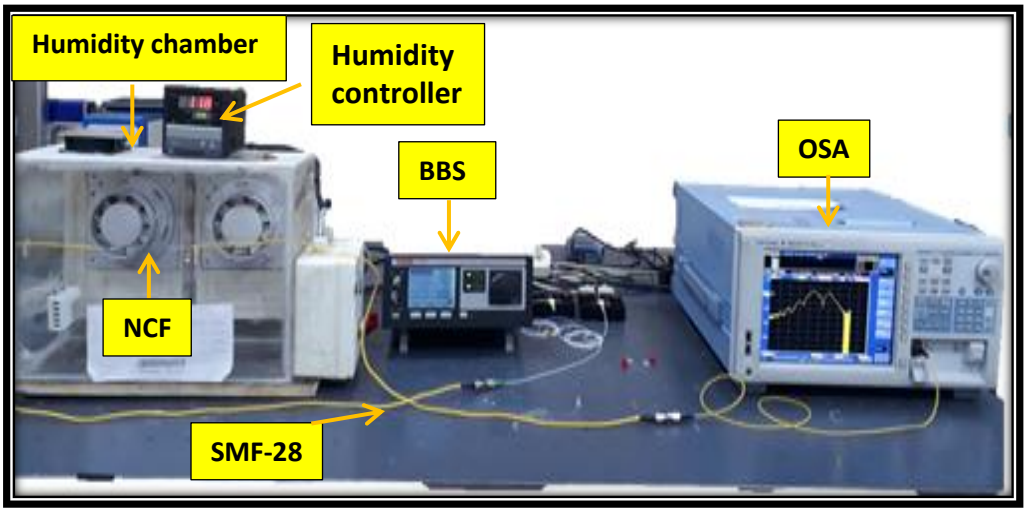

Figure (2.3)The photographic picture for the SNCS humidity sensor set up.

2.2.1 Broadband source (B.B.S):-

In this work, a butterfly-packaged Super-Luminescent Diodes (Thorlabs SLD1550s-A1) with 1400-1600 nm emission range has been used as a broadband light source, as shown in figure (2.4). This source has an excellent power, near-Gaussian with flat-top optical spectrum as well as low-ripple.

This device is constructed into a 14-pin butterfly package with a combined thermoelectric cooler (TEC) and a thermistor to confirm the stability of the output light. The output is coupled into an SMF that ended with a 2.0 mm fine knob FC/APC adapter.(Appendix A)

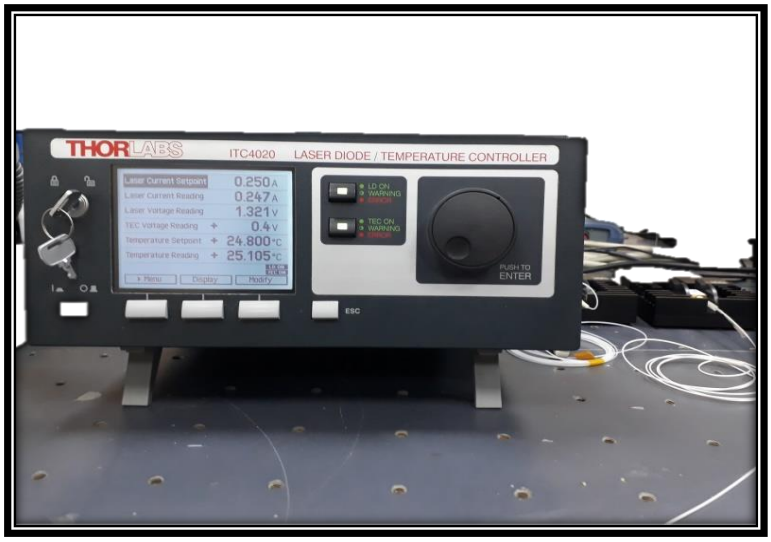

Figure (2.4) Photo-image of Broadband source (B.B.S)

2.2.2 Single - Mode Fiber (SMF-28):-

(SMF-28) is considered the "standard" optical fiber for submarine, cable television, telephony, and private network applications in the spread of video, data and\ or voice services. the capacity of fiber aimed at carrying the information is the highest in the transmission window of 1310 nm (the wavelength region), and also the dispersion in this wavelength

region is the lowest. The SMF-28 has robust geometric characteristics such as low attenuation and high strength. Corning single mode fiber can be used for excellent deliver performance and high precision [Appendix B]. Top view of SMF-28 under a microscope shown in figure (2.5), which shows the quality of the cleaved end of SMF.

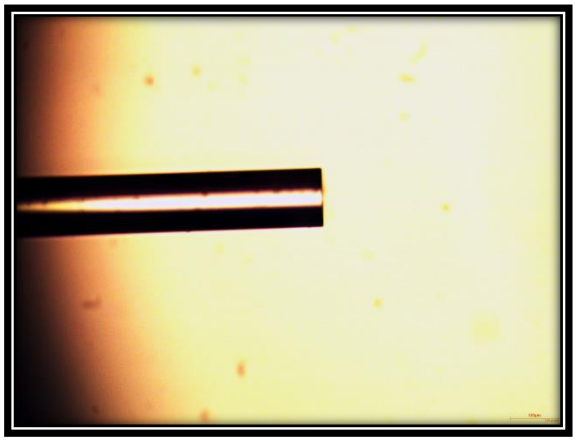

Figure (2.5) Top view for the SMF under microscope with magnification power (10x)

2.2.3 No-core fiber (NCF) (Thorlabs):-

NC fiber (FG125LA from Thorlabs Company) has been used in this experiment. It considers special type of multimode fiber with outer diameter 125 µm could be spliced to the ends of SMF.

Moreover, NCF consider a special type of multi-mode fiber when it's spliced to the ends of SMF . NCF operated with a wide wavelength range with return loss > 65 dB. NCF has a different operating wavelengths at different refractive indexes, where NCF has RI about 1.444 at wavelength 1550 nm. The optical specifications of NC fiber are given in the table (2.1) [Appendix C].

Table (2.1): Optical specifications of NC Fiber [from Appendix C].

Wavelength range (nm)	**400-2400**
Glass Diameter (µm)	125±1
Coating Diameter (µm)	250±5%
Operating Temperature C °	-40 to 85
Glass Refractive index and operating wavelength	1.444 @1550 nm 1.467287 @ 436 nm 1.458965 @ 589.3 nm 1.450703 @1020 nm

2.2.4 Optical spectrum analyzer (OSA):-

Optical spectrum analyzer OSA (YOKOKAWA, Ando AQ6370) has been utilized to monitor the variation in the interference spectra of the OFHS. It is a precision device used to measure and displays the distribution of power of the optical source over a certain wavelength span. And it trace displays the wavelength in the horizontal scale and the power in the vertical scale. figure (2.6) shows the photograph of OSA used in the experiment.

The main properties of OSA are tabulated in table (2.2).

Table (2.2): OSA Characteristics used to perform this work.

Wavelength range	600 nm to 1700 nm
High wavelength accuracy	± 0.01nm
Wide Dynamic range	78 dB typ.
Fast measurement	0.2 sec. (100nm span)
Wide level range	+20 dBm to -90 dBm
High wavelength resolution	0.02 nm
applicable to	SMF, MMF Patch cable fibers

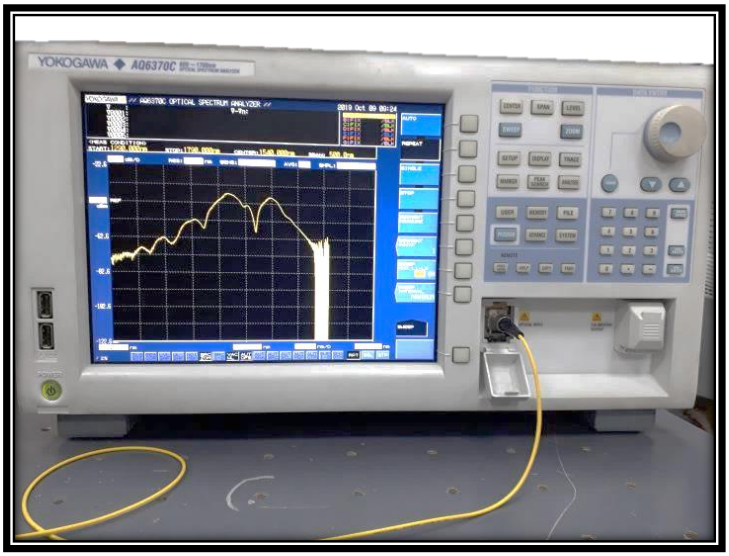

Figure (2.6): Photo-image of optical spectrum analyzer (OSA).

2.2.5 The Humidity Chamber:-

To study the humidity response of the SNCS sensor, a sealed cuboid-shape chamber made from Polyvinyl chloride (PVC) plastic with dimensions (length =40cm,height= 27cm, and width=17cm) is used. The chamber has three fans. One of them is used to pump dry air form container with silica gel to accelerate the humidity diffusion in the chamber access, the second fan is used to pump a wet air from a container filled with deionized water heated by 70watt heater, to supply the humidity to the chamber. The last fan is used for chamber discharge and cooling, as illustrates in figure (2.7). A calibrated electronic humidity (XMT9007-8 temperature & humidity control instrument) is used for monitoring the temperature and humidity inside the chamber.

(a) **(b)**

Figure (2.7) Photo-image of the humidity chamber (a) front view (b) top view

2.3 Principle of Operation

The sensor structure is composed of an NCF fiber spliced between two SMFs. When the incident light propagates from the input SMF to NCF, the higher-order modes will be exited. During propagation along the NCF part, these modes will experience interference which leads to a multimode interference (MMI) [61]. In order to have a self-image right at the output of the SMF, the length of the NCF has to be precisely chosen. The MMI effect has been previously studied and the length of the NCF can be given as [62-63].

$$\boldsymbol{L_{\mathrm{NCF}} = m\left(\frac{3L_{\pi}}{4}\right)} \quad \textbf{With m = 1,2,3,…} \qquad (2.1)$$

Where m refer to self-imaging number and L_{π} is the beat length,

$$\boldsymbol{L_{\pi} = 4\, n_{\mathrm{NCF}}\, D_{\mathrm{NCF}}/3\lambda_0} \qquad (2.2)$$

According to MMI theory, the interference wavelength can be given from the following formula [63]:

$$\boldsymbol{\lambda_0 = m\left(\frac{n_{\mathrm{NCF}}\, D_{\mathrm{NCF}}^2}{L_{\mathrm{NCF}}}\right)} \qquad (2.3)$$

Where $D_{NCF,}$ $L_{\mathrm{NCF},}$ n_{NCF} and m are the diameter of NCF, length of NCF, the effective refractive index and interference number, respectively.

The performance of the proposed sensor is essentially related to the variation in the refractive index of the surrounding medium of NCF. By changing the RH, the RI around the NCF region would change leading to a shift in the output wavelength [88].

2.4 Experimental Procedures

Experimental procedure follows two steps to fabricate an optical fiber humidity sensor based on SNCS fiber structure, it is as follows:

2.4.1 Singlemode-NC fiber-Singlemode (SNCS) structure.

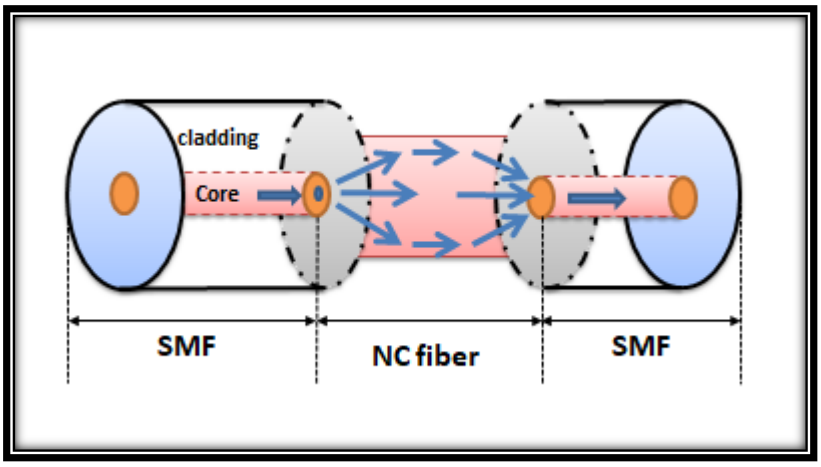

Figure 2.8 Schematic of the SNCS structure.

SNCS sensors have been designed and constructed by cleaving and splicing NCF (FG125LA Thorlabs, 20 mm in length) between two conventional optical fiber (SMF-28), as shown in figure (2.8). The SMFs have a core and clad diameters of 9 µm and 125 µm, respectively. While the NCF has the same cladding diameter of 125 µm, then tests the optimum diameter with

different lengths of the NCF. After that, the optimum length and diameter were selected for coating with Al_2O_3-PVA.

2.4.2 NCF and SMF cleaving.

In order to prepare the NCF and SMF for fusion splicing, Firstly cleaving fibers was done by removing the protective polymer coating before splicing to minimize splicing loss and obtain good splicing characteristics. Removing the protective polymer layer could be done by alcohol or mechanical stripping. In this experiment mechanical Fiber Stripper (JIC – 375 Tri – Hole) was used to remove the polymer layer. Secondly, the optical fiber cut with the right angle using the cleaver machine (CT-30) (Fujikura).

Figure 2.9: Cleaver (CT-30)

The optical fiber cleaving allows the clamping of the fiber into the specified position, also presented to make an optical fiber flat face and perfectly smooth. By putting the edge of the optical fiber above the cutting blade of the cleaving machine, a cleaved end surface of optical fiber with 90^0 angle and flat cleaved surfaces can be obtained. Finally, the fiber was cleaned

with wet wipe or alcohol or other any solvent. figure (2.10) Top view of NCF under a microscope, which shows the edges of the fiber were well-cleaved.

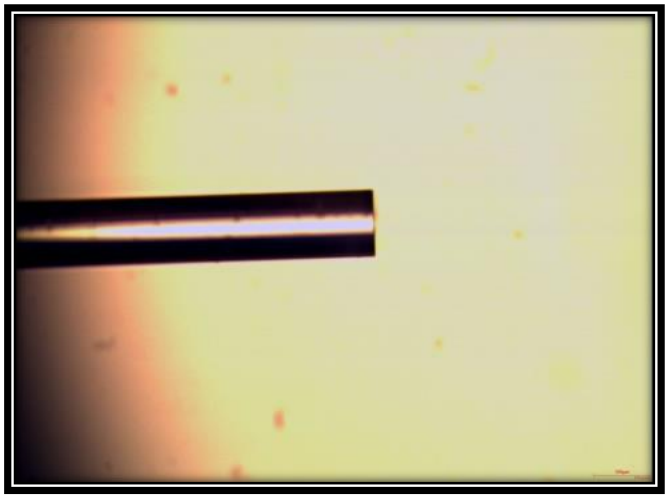

Figure (2.10): Microscope images of NCF end after cleaving.

2.4.3 NCF and SMF splicing.

Splicing is the process of connecting two segments of optical fibers like NCF and SMF. In this experiment, Fusion splicer from Fujikura (FSM-60S) splicing machine, shown in figure (2.11), is used in AUTO_MODE to fusion splice the SMF have core and cladding refractive index 1.451 and 1.444 respectively. The NCF has a diameter of 125 with 1.444 refractive index, So the same refractive indices and diameter for the SMF and the NCF. This compatibility made the splicing easier and homogeneity.

Figure (2.11) Optical fiber arc fusion splicer type (FSM-60S).

the NCF ends with different diameters and lengths is cleaved according to a certain length range and both ends are spliced with two standard SMFs-28 using electric arc technique. A fusion splicer with automatic mode was used to form SMF-NCF-SMF (SNCS) structure with a reiterated arc discharge technique to minimize the splicing loss as much as achievable as shown in figure 2.12. In general, fusion splicing based on electric arc technique has been most utilized and has been much best created than the others techniques.

Figure (2.12): Fusion splicer process between NCF and SMF.

A section of SMF-28 of 1 m-length and 125 μm diameter was spliced to the NCF of a 20 mm-length and 125 μm diameter on from both sides using the AUTO MODE function in the fusion splicer menu (Fujikura FSM-60S) with good mechanical strength and low loss. The splicing loss was about 0.01 dB for each splicing region, where prepared different diameter of NCF by using chemical etching with fixed length, after study the influence of the diameter, the lengths of NCF recalculated to be (40, 60) mm.

The standard steps to fusion splicing are:

- Remove any outer protective polymer coating from the fiber using stripper.
- Using clipper to cleave ends of optical fibers at right angles with 90^{o} then cleaned the fiber ends with lens tissue and alcohol.
- Adjust the optical fiber ends in the V- groove in the fusion splicing machine accurately with a small gap in between the optical fibers.
- Press the set mode to start the arc fusion and then protect the splicing region.

2.4.4 NCF etching procedures

One of the mechanisms used to improve the sensitivity of SNCS structure is the chemical Etching process to decreasing the NCF diameter. The NCF was reduced by using 40% diluted hydrofluoric acid (HF) as an etchant on different diameters NCF of (100, 75 and 50)μm respectively. The purpose of optical fiber etching to allow more interaction of propagating light with relative humidity.

Two important factors were carefully adjusted to control the diameters of the NCF which are; etching time and average etching rate. The etching time

needed to decrease of NCF diameter from 125µm to 100 µm, 75µm and 50µm were (12, 23, 35) min, respectively, such that the average-etching rate was about 2.14 µm/min at room temperature.

In this work, The SNCS fiber structure fixed on both sides and the NCF segment emerged in the hydrofluoric solution HF (~ 40%) using a quartz U-shape groove. NCF diameter was reduced to 50µm by controlling the etching time and average etching rate. In this step, the NCF length was fixed on 20 mm and then, the best diameter with different lengths (40,60)mm were , tested .

To see top view NCF after the etching process, a transmission optical microscope from (Euromex Company, Holland) was used, as shown in figure (2.13). This microscope has different magnification power (4 X, 10 X, 40 X and 50 X).

Figure (2.13) The Transmission Optical Microscope

figure(2.14) shows microscopic images of NCF etching with different diameters imaged under an optical microscope.

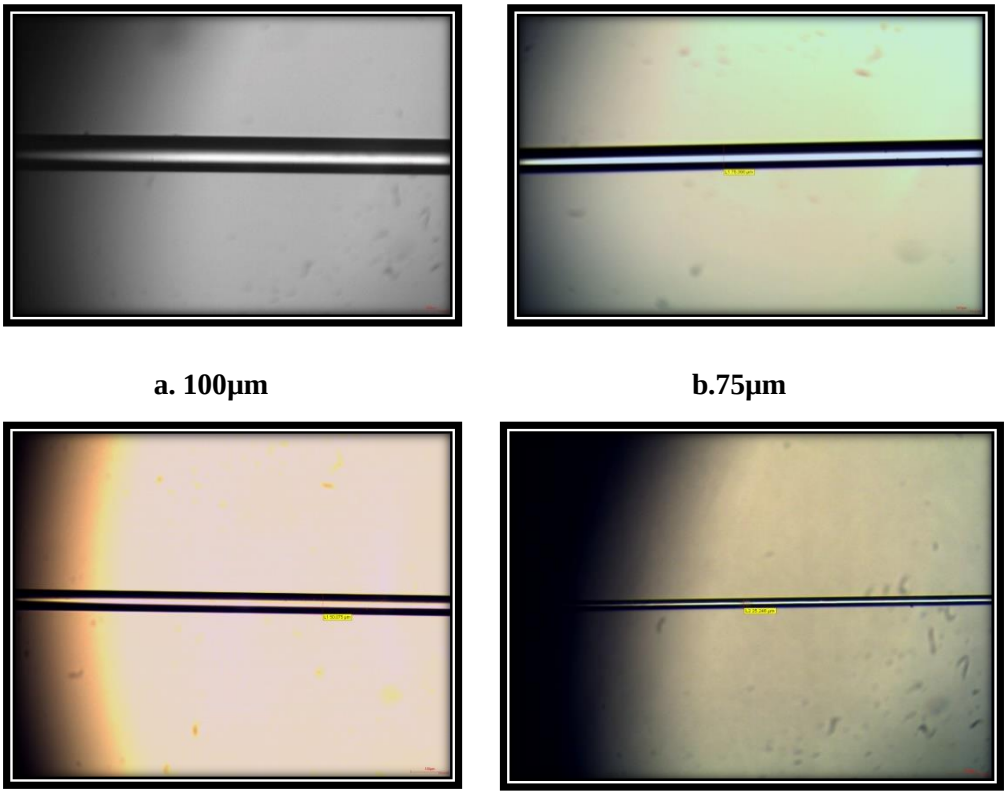

a. 100µm **b.75µm**

c. 50µm **d. 25µm**

Figure (2.14) Microscopic image of NCF diameter etching (a)100 µm (b)75 µm (c)50 µm (d)25 µm with (10X)

also figure (2.15) shows the scanning electron microscopy (SEM) image of the etched NCF with 50µm diameter at different magnification.

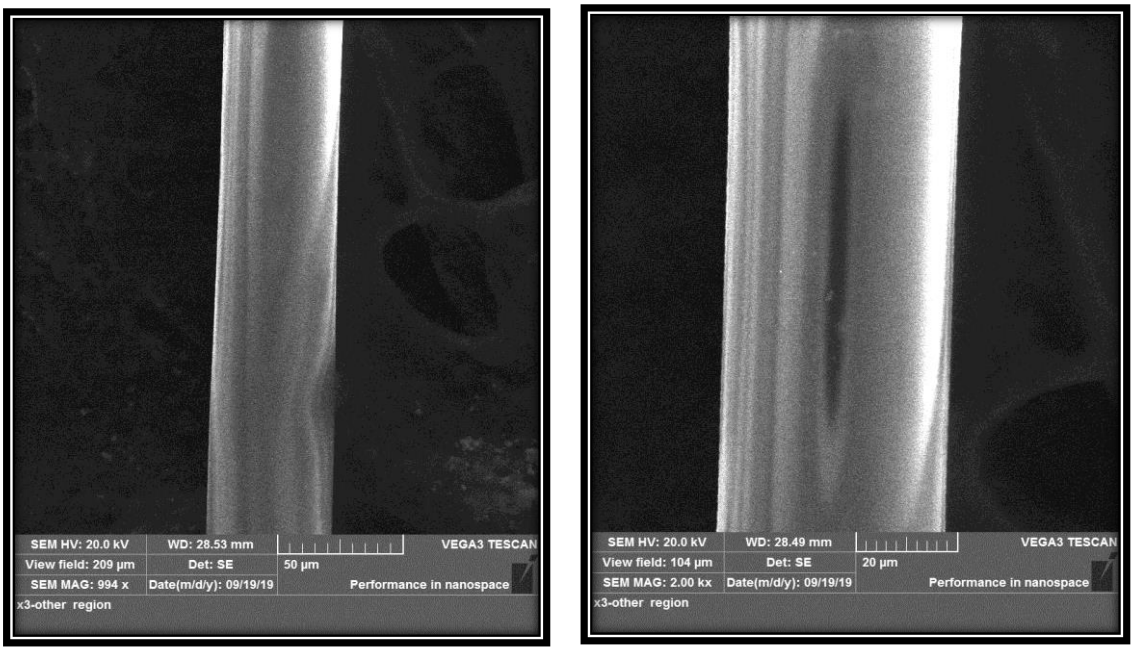

(a) **(b)**

Figure (2.15): The SEM image of the etched NCF with 50 µm diameter at different magnification of (a) 50 µm and (b) 20 µm

2.4.5 Preparation of Al_2O_3-PVA composite

After fabrication the SNCS fiber structure with the optimum NCF length and diameter, Al_2O_3 NPs embedded in PVA polymer as a sensitive film was coated on the surface of NCF using the cast-drop and evaporation technique. The properties of Al_2O_3 nanoparticles are presented in Appendix (D).

figure (2.16) shows The SEM image of the Al_2O_3 NP_s which are around 20 nm in size (Nano-shell), The coating process started with the preparation Al_2O_3-PVA solution, Firstly, the PVA solution was prepared by mixing 10 g into 100 ml deionized water. Then, the solution was heated at 90 °C and mixed thoroughly using magnetic agitation for 1 h. The samples were left to cool at room temperature. Then, 25 mg of Al_2O_3 NP_s were added to 25 ml of the PVA solution with a weight ratio of 1:1. The mixture was stirred at a moderate rate with a magnetic stirrer time for 90 minutes to obtain a homogenous solution. In order to remove the effect of bubbles, the solution

was let to settle for 2 h. Finally, the NCF segments were coated with Al_2O_3-PVA composite and left to dry for 5 h.

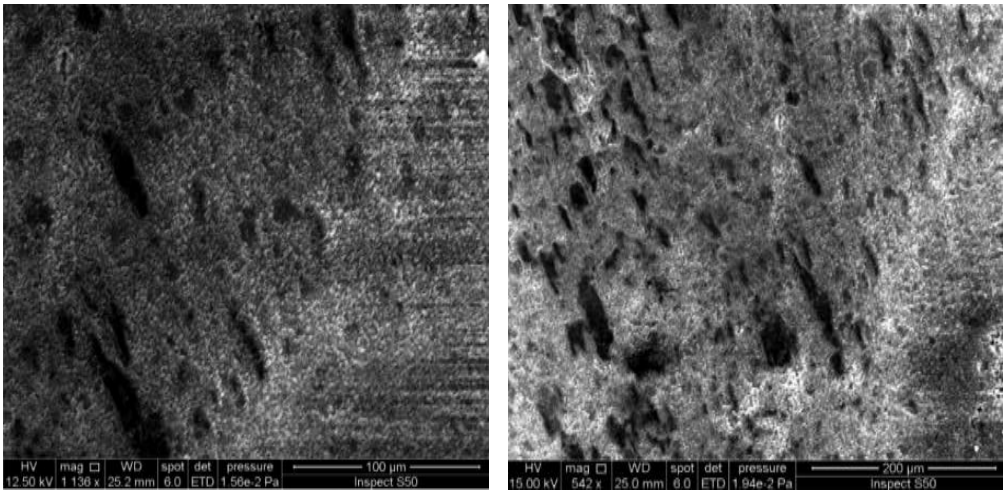

(a) **(b)**

Figure (2.16) SEM images for Al_2O_3 NPs at a magnification of (a) 100 µm and (b) 200 µm .

The Al_2O_3-PVA composite and coating process are shown in figure (2.17), the thickness of the coating after different coating numbers was about ~8 µm, also could control the size of the film when the SNCS structures coated with different concentrations of Al_2O_3-PVA and different coating numbers.

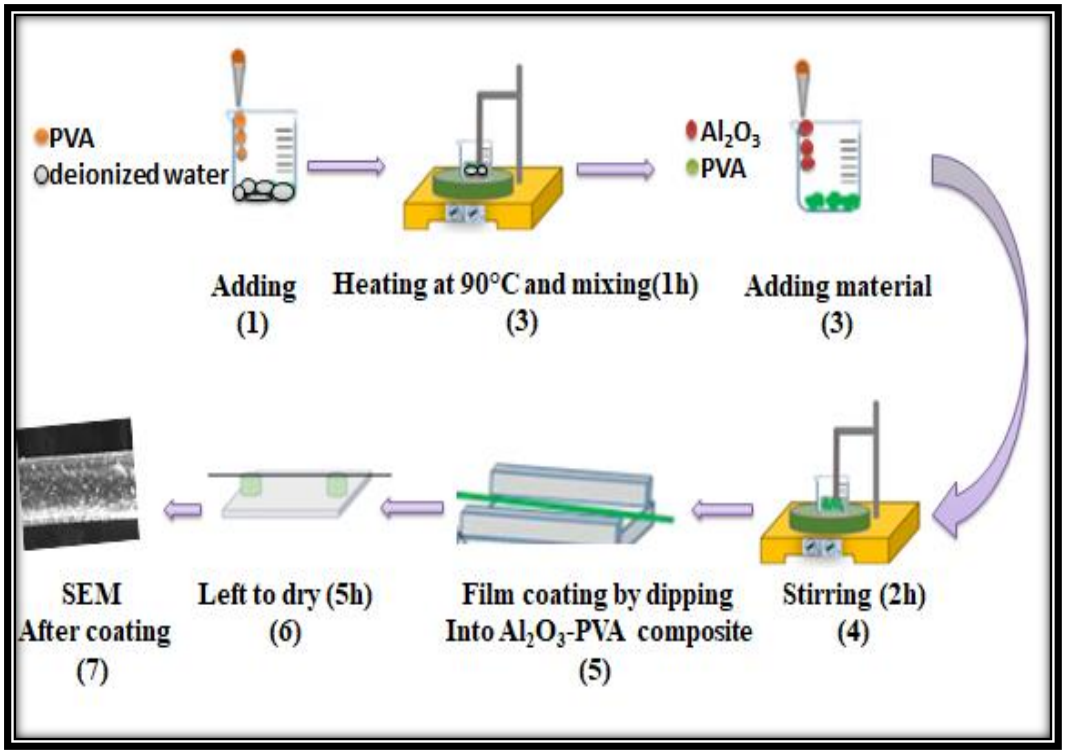

Figure (2.17): The preparation Al_2O_3-PVA and coating process.

2.5 Optical fiber humidity sensors based on multimode interference using SNCS setup:

The SNCS fiber structure was designed and fabricated as stated in section (2.4.1), the sensor was tested by studied the influence of two parameters, the length and the diameter of NCF segment . The following the procedures to study the effect of those parameters were illustrated in this section on the optical fiber humidity sensor sensitivity. the sensor was fabricated using fusion splicing of three different lengths of NCF: 2, 4 and 6 cm in-between two SMFs. The resultant SNCS were tested as optical fiber humidity sensor when the RH changed between 30% and 100%. The NCF diameter was changed from 125 µm to (100, 75, 50 and 25) µm by chemical etching. The influence of each diameter on the optical fiber humidity sensor sensitivity was tested.

2.6 The influence of the NCF length on the sensitivity:-

A transmission type SNCS in which the two ends of (6 cm, 4 cm, 2cm) length of etched NCF was fusion spliced to lead-in and lead-out SMFs , The humidity response of the sensors was studied by placing the SNCS fiber structure in a controlled environment chamber which was a cuboid-shape sealed and connected from one side with Broad Band Source (BBS) (Thorlabs) with wavelength range 1500-1600 nm and from the other side with an optical spectrum analyzer (OSA) with a resolution of 0.02 nm, and the RH varied between 30% and 100% as shown in figure (2.2) with maintaining the temperature at 25 C^{o} and The result wavelength shift and sensitivity was recorded using OSA.

2.7 The influence of the NCF diameter on the sensitivity:-

The SNCS structure with 2 cm of the NCF length was etched from 125μm to (100, 75, 50, and 25) by chemical etching, then the SNCS fiber structures were tested as optical fiber humidity sensor when the RH changed between 30% and 100%. The influence of each diameter on the sensor sensitivity was tested. After testing the sensor, the NCF has been coated with a thin layer of Al_2O_3-PVA which acts as a cladding for NCF instead of air with optimum length and diameter for furthermore enhancement of the sensitivity.

2.8 The Rise Time Calculation:-

Rise time is the time required for the signal to increase from low value (10%) to high value (90%) [72].The response of the sensor is measure to the changes in RH from 30% to 100%, for an SNCS fiber structure coating with Al_2O_3-PVA thin film with optimum NC fiber length and diameter.

Chapter Three

Results and Discussion

3.1 Introduction

This chapter presents the results, discussion, conclusion, and future work of the fabricated transmission type MZI as an optical fiber humidity sensor based on the SNCS fiber structure. The influence of different lengths and diameters of NC fiber and for pare and coated NC fibers with different humidity values were studied.

To establish and implement a relative humidity sensor, The experimental setup is settled based on wavelength. The results of the experimental setups were discussed. The sensor sensitivity was calculated by dividing the experimentally measured SNCS fiber structure response to the relative humidity. Also, the rise time of the sensor was calculated for this sensor.

The experiments were carried out by using an optical spectrum analyzer (OSA) at 0.02 nm resolution and broadband source (1500-1600) nm. All the results in this work were taken under conditions of the scientific laboratory. The temperature of the room was 25˚C and normal atmospheric pressure

3.2 Transition Spectra and stability for SNCS fiber

The schematic diagram of the experimental setup was shown in fig (3.1) (a) and (b). Firstly the transmission stability of B.B.S was checked to ensure later accurate measurements. The first side of SMF was connected to OSA and the other side to the B.B.S as shown in figure (3.2 bold red curve). The next step was carried out with SNCS fiber structure at 125 µm NCF diameter and length 20mm. When the SNCS fiber structure with NCF diameter of 125µm and length of 20mm connected to the B.B.S, it worked as a band-pass filter where some wavelength modes were filtered out due to the MMI effect as shown in figure (3.1 black bold line).When the transmitted light propagates from SMF to NCF multiple high order modes are transmitted and exited, these

modes propagate along the direction of NCF and interfere with another, causing rise in a multimode interference (MMI) and re-emerged into SMF.

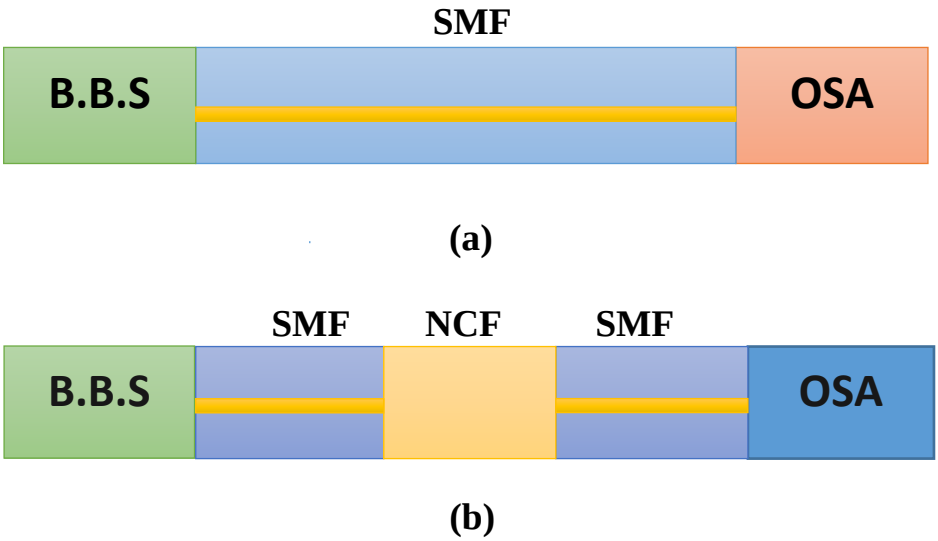

Figure (3.1) schematic of experimental setup (a) SMF (b) SNCS.

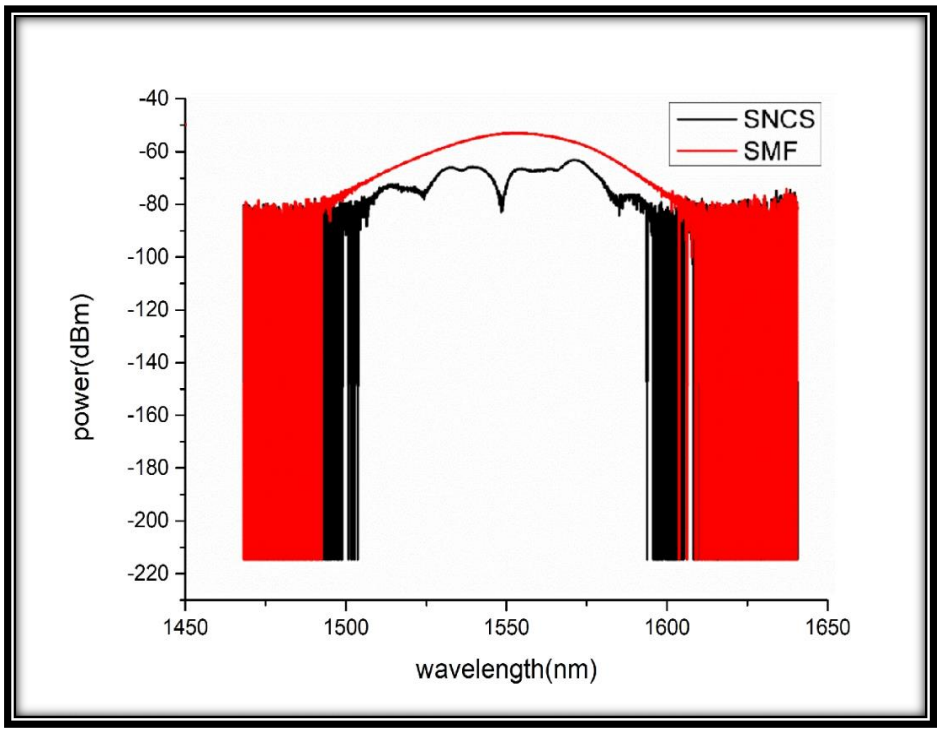

Figure (3.2): Output Specta of B.B.S of SMF and SNCS.

3.3 The Influence of NCF Diameter on the OFH sensor.

The influence of NCF Diameter on increase the sensing sensitivity was investigated by using different diameters of NCF with fixed length (20mm), The SNCS structure was fabricated by using fusion splicing of NC fiber in-between two SMFs, which was operated by AUTO MODE; The etching process executed by emerging the NCF in HF acid to decrease the outer diameter of NCFs from 125 µm to 100, 75, 50 and 25 µm respectively. The transmission spectra response of the etched NCFs with the change of external RH was recorded.

3.3.1 The 125 µm NCF diameter as OFHS

Firstly, the response of the SNCS fiber structure without etching (with 125 mm of NCF diameter) to the variations of the RH was investigated. the fabricated sensor was placed in a relative humidity chamber equipped with an electronic humidity sensor (XMT9007-8 humidity control instrument) for observing the humidity changes from 30% to 100% inside the chamber while the temperature inside the chamber was kept in the range between 25 to 30°C. Figure 3.3 shows the transmission spectra response of the proposed RH sensor, where the sensitivity attained was 0.128 nm/%RH. The excited evanescent waves will interact with the surrounding RH and introduce the change in the output spectrum. Also, from this figure, it can be noticed that the transmission spectra shifted towards longer wavelengths at each increase in RH.

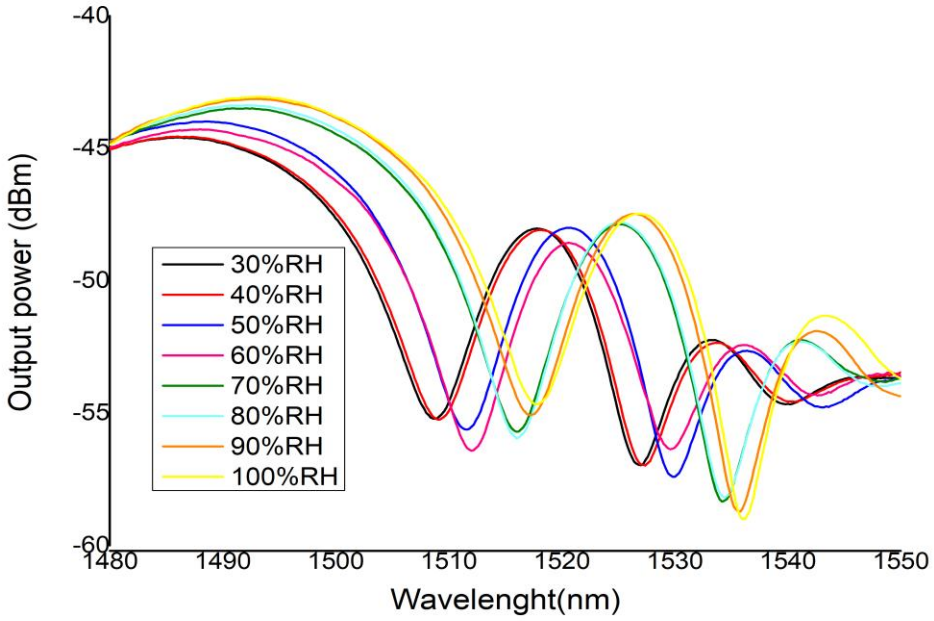

Figure 3.3: The transmission spectra of the SNCS sensor with RH variation from 30% to 100% with a diameter of 125 µm.

3.3.2 The influence of 100µm NCF diameter on the OFHS.

The NCF with 100µm was etched by submerging in HF acid to 12 min; the transmission spectra for SNCS fiber sensors of 100µm are depicted in figure (3.4) where the RH changes 30% RH to 100% RH. It shows that the NCF diameter will directly affect the sensor sensitivity. When the RH increased from 30% to 40% the dip in the spectrum shifted from 1492nm as shown in figure (3.4 black bold line) to 1495.8nm (3.4 red bold line). The transmission spectra shifted towards red when the refractive index increased from 1 in air to 1.333 in the water. The wavelength shift was continued in red direction when the RH was increased. the sensitivity attained of SNCS fiber structure with 100µm NCF diameter was 0.164 nm/%RH. The reduction in NCF diameter from 125µm to 100µm contribute in an enhancement of the sensor sensitivity that due to the enhanced evanescent field.

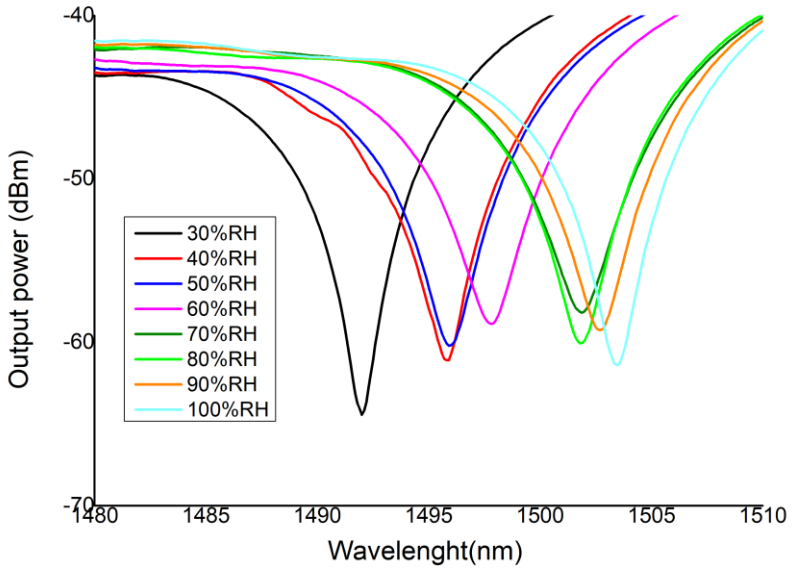

Figure 3.4: The transmission spectra of the SNCS sensor with RH variation from 30% to 100% with a diameter of 100µm.

3.3.3 The influence of 75µm NCF diameter on the OFHS .

To reducing the NCF diameter to 75µm, The NCF chemically etched by submerging in HF acid about 23 min. a fixed NCF length of 20mm was used in the SNCS structure. figure (3.5) shows the wavelength shift dependence on the RH for NCF segments at 75µm when the RH increased from 30%RH to 100%RH. The position of the transmission dip was red-shifted around 13.6 nm as the surrounding RH increases. Also from this figure, it's could indicate that there are longer wavelength shifts with humidity variation when the NCF diameter was reduced to 75µm. The wavelength sensitivity of the SNCS fiber sensor with 75µm NCF diameter was 0.194nm/%RH.

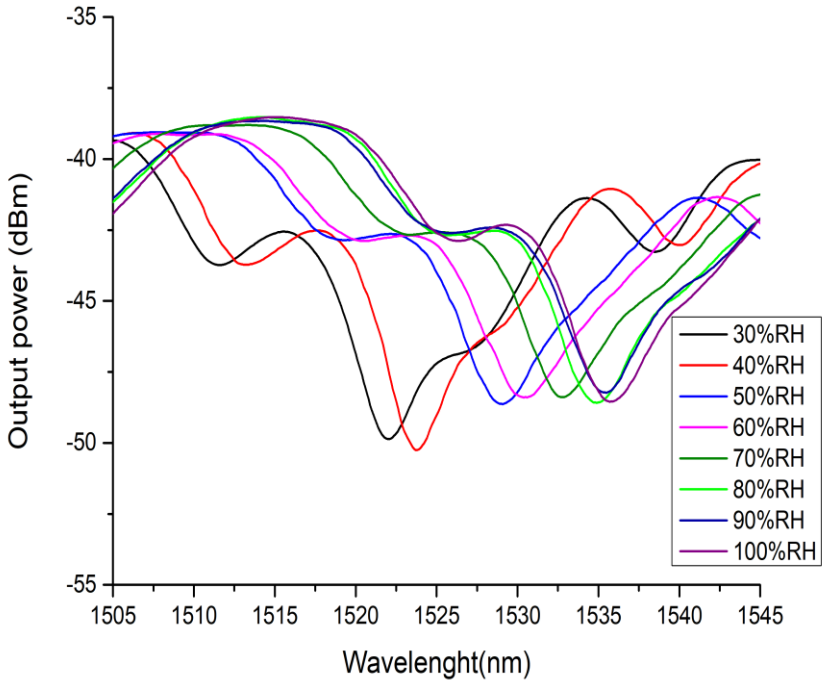

Figure 3.5 The transmission spectra of the SNCS sensor with RH variation from 30% to 100% with a diameter of 75µm.

3.3.4 The influence of 50 µm NCF diameter on the OFHS sensitivity

From figure (3.6), the SNCS sensor structure with the diameter of 50 µm shows the larger wavelength shift when the RH increased 30%RH to 100%RH than that of 125µm basic structure. The results indicate the RH sensitivity was enhanced from 0.128nm/%RH to 0.262nm/%RH as NCF diameter was reduced from 125 µm to 50 µm. Since decreasing the diameter allows more interaction of evanescent waves with environment humidity [89].

The NCF diameter of 50 µm has the highest sensitivity compared to other diameters, the sensitivities attained were 0.128 nm/%RH, 0.164 nm/%RH, 0.194 nm/%RH and 0.262 nm/%RH for (125, 100, 75, and 50 µm) respectively, for the same NCF length(20mm).

Consequently, the diameter of 50 µm has been selected as the optimum NCF diameter for the sitting sensor structure. figure (3.7) illustrates the

wavelength shifts of the RH sensor to the variations of the relative humidity from 30% to 100% with different NCF diameters (125, 100, 75, and 50 μm). We noticed that the RH sensitivity has been enhanced when reducing the NCF diameter. It should be noted that the etched NCF with diameter of 25μm was not be considered as an influenced diameter, due to difficult to handle and high losses in the output spectrum.

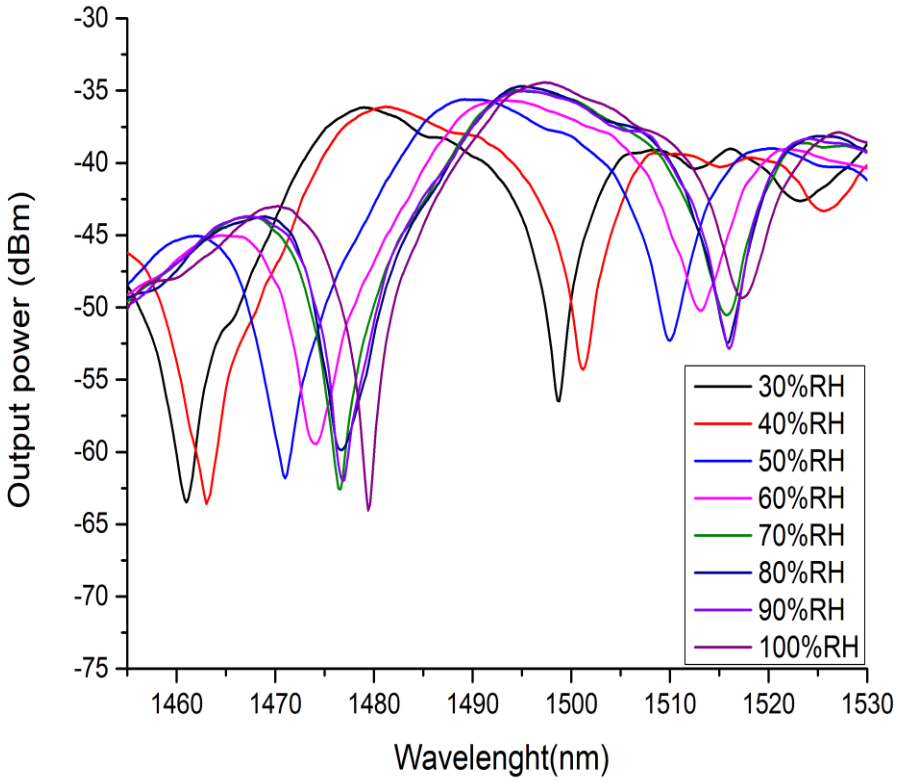

Figure 3.6 The transmission spectra of the SNCS sensor with RH variation from 30% to 100% with a diameter of 50μm and 20mm length.

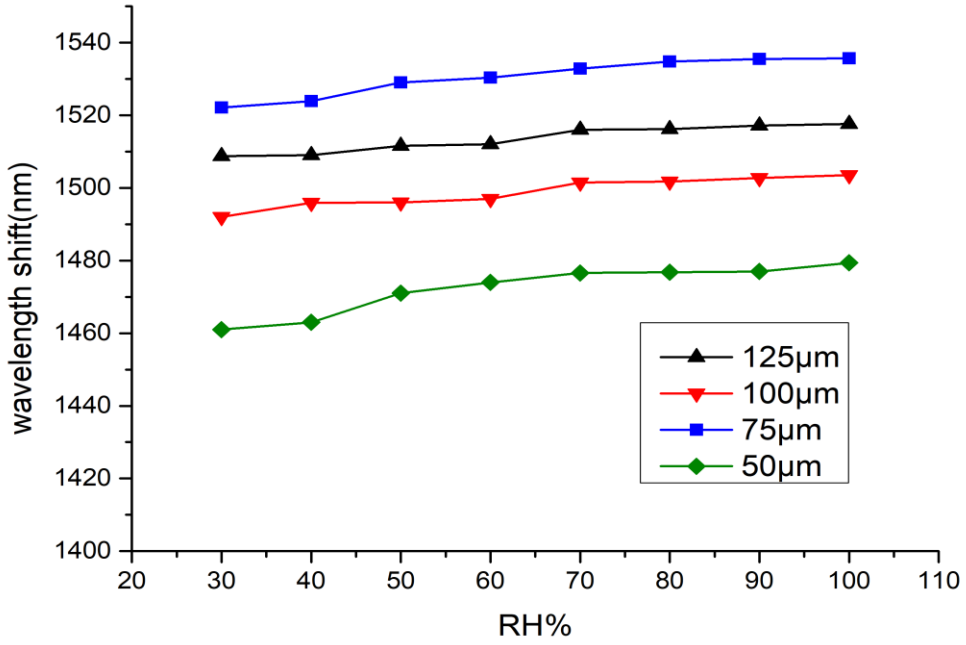

Figure (3.7): The response sensors to variations in RH from 30% to 100% with different NCF diameter

3.4 The Influence of NCF length on the sensitivity of OFHS

The influence of NCF length on OFHS sensitivity was studied in this experiment by using different lengths of NCF with a fixed diameter of NCF at 50 μm. SNCS fiber structure was prepared with diameter 50μm and three different lengths (60,40,20) mm, figure (3.6), It's shown that the SNCS structure with a diameter of 50 μm NCF and a length of 20mm will directly affect on the sensor sensitivity. Then relative humidity was tested with different each NCF lengths (40, and 60) mm as shown in figure (3.8) and figure (3.9). As expected, the sensor shows the higher sensitivity at NCF length of the 20 mm, which shows shifted towards longer wavelength at each increase in RH compared to (40,60) mm, this is due to the connection between the SMF and NCF, the constructive interference modes occur in SNCS structure due to the multimode interferometer (MMI).

The sensitivities attained were 0.179 nm/%RH, 0.2 nm/%RH and 0.262 nm/%RH for (60, 40 and 20 mm) respectively. Consequently, the length of 20mm has been selected as the optimum NCF length for the sitting sensor structure. figure (3.10) illustrates the wavelength shifts of the RH sensor to the variations of the relative humidity from 30% to 100% with different each NCF length (20,40and60 mm). We noticed that the RH sensitivity has been enhanced when reducing the NCF length, reflecting the effect of NCF length on sensitivity.

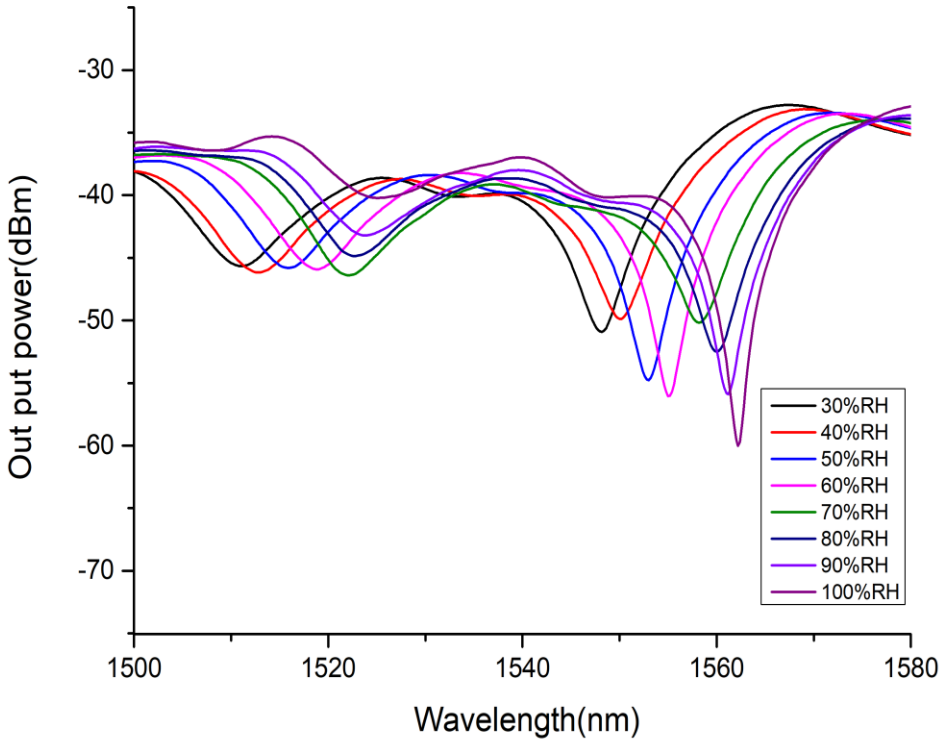

Figure (3.8) the transmission spectra response of the OFHS as a function of RH for 40mm length.

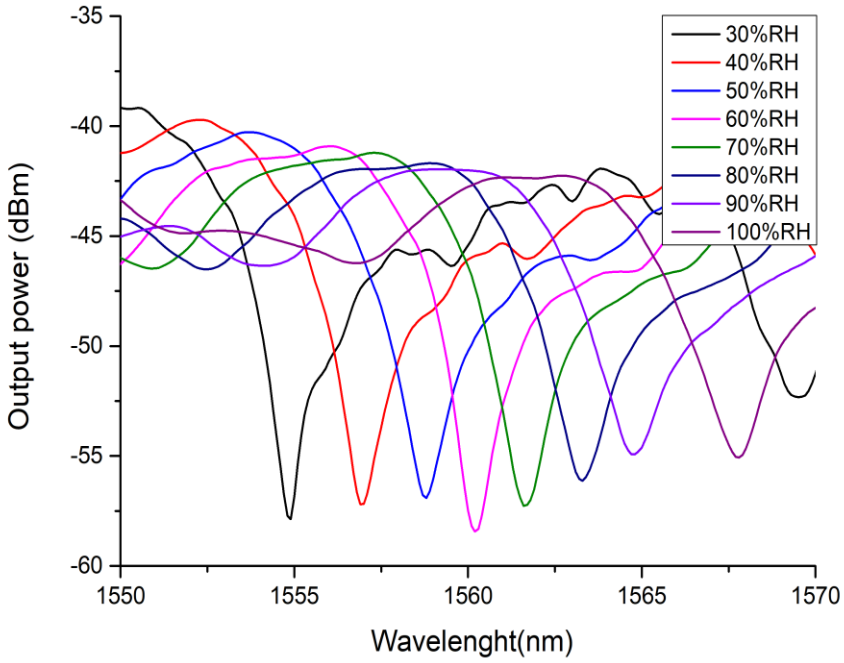

Figure (3.9) the transmission spectra response of the OFHS as a function of RH for 60mm length

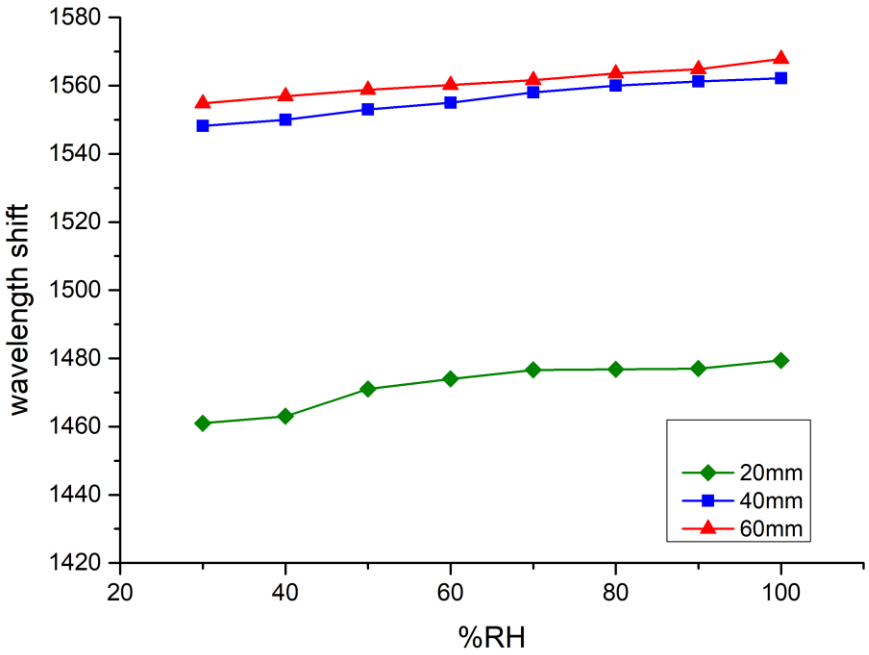

Figure (3.10): The response sensors to variations in relative humidity from 30% RH to 100% RH with different NC fiber length

3.5 The influence of coating on OFHS sensitivity

In order to enhance the sensitivity of the fabricated sensor further, Al_2O_3- PVA was selected as the sensitive film coating for 50 µm and 75 µm NCF diameter. The strength of the light interaction with the coated Al_2O_3 was remarkably enhanced at reduced waist diameter, and consequently, the sensor became more sensitive to RH changes. figure (3.11) (a, b) illustrates the SEM images of the etched NCF coated with Al_2O_3 NPs at a diameter of 50 µm at different magnification, the coated layer is homogeneous.

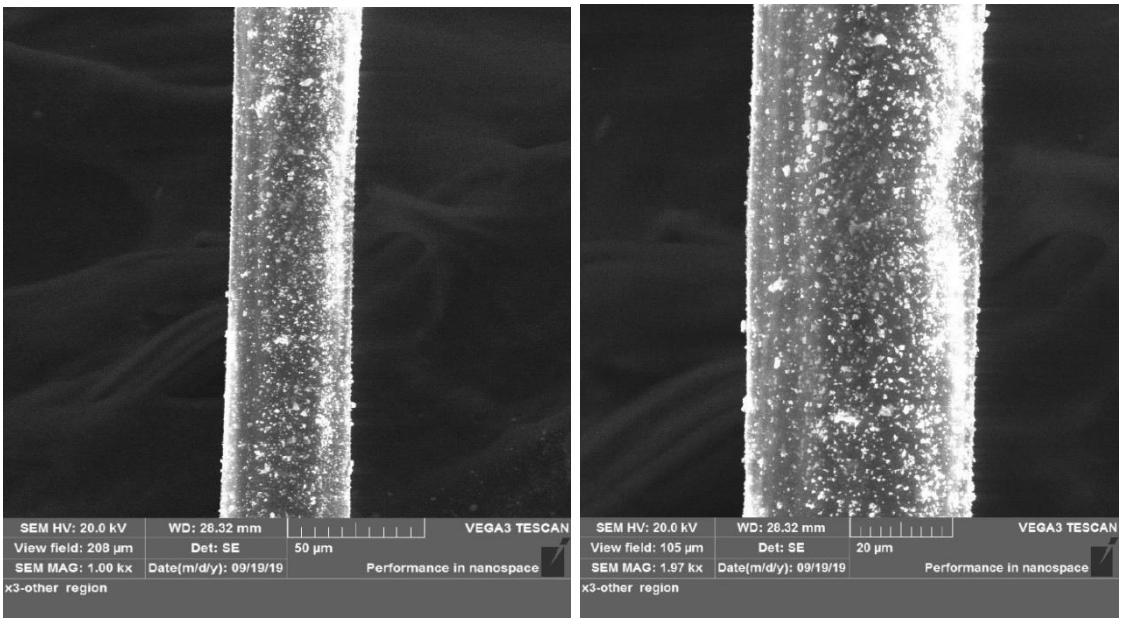

(a) **(b)**

Figure (3.11): The SEM images of the etched NCF coated with Al_2O_3-PVA thin film at a diameter of 50 µm with different magnification of (a) 50 µm (b) 20 µm

figure (3.12) and figure (3.13) shows the wavelength shift dependence on the RH for both coated NCF segments at 75 µm and 50µm when the RH changes 30%RH to 100%RH. The position of the transmission dip was red-shifted around 38.9 nm as the surrounding humidity increases. During this process, more water molecules were diffused into the Al_2O_3-PVA film which can effectively modify the film refractive index [89]. Moreover, PVA is known to have good permeability and a high swelling ratio [90-91]. The fitted curve shows that the sensitivities of the proposed sensor are 0.587nm/% RH with

an R^2 value of 0.9812 and 0.295nm/% RH with an R^2 value of 0.96 for NCF diameter of 50 µm and 75 µm, respectively as shown in figure (3.14) and figure (3.15). As expected, the sensitivity was higher at the NCF diameter of 50 µm compared to 75 µm due to the enhanced evanescent field. The strength of the light interaction with the coated Al_2O_3 was remarkably enhanced at reduced waist diameter, and consequently, the sensor became more sensitive to RH changes.

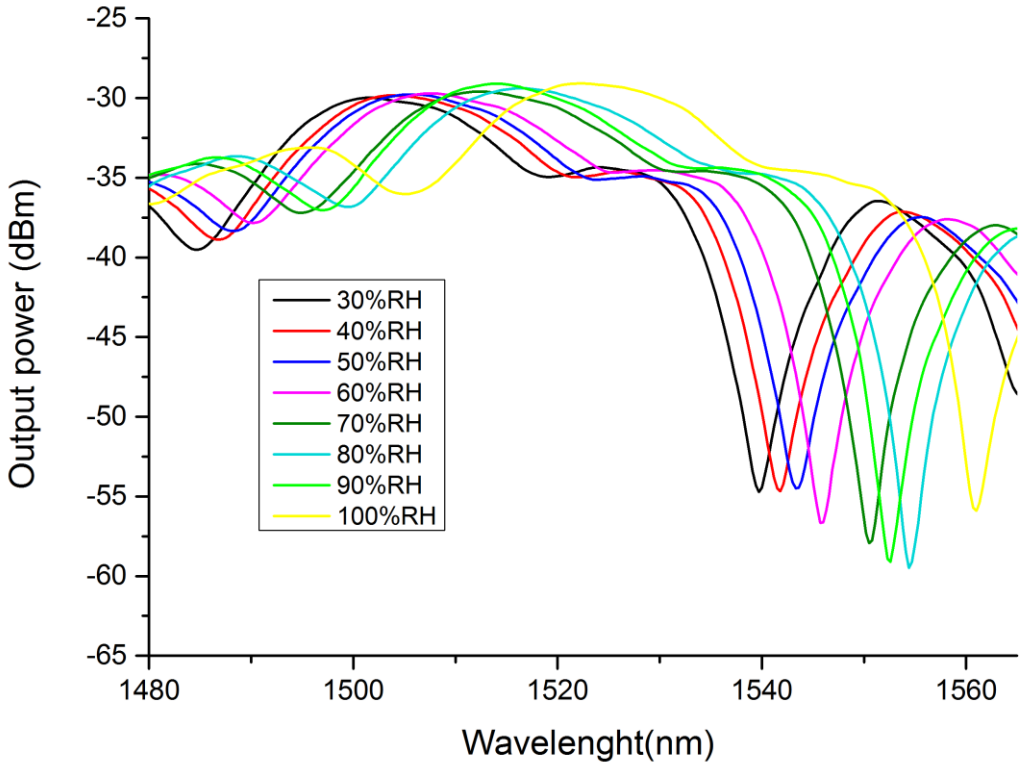

Figure (3.12): Transmission spectra of the SNCF sensor with relative humidity variation from 30% to 100% with diameters of 75µm coated with Al_2O_3- PVA thin films

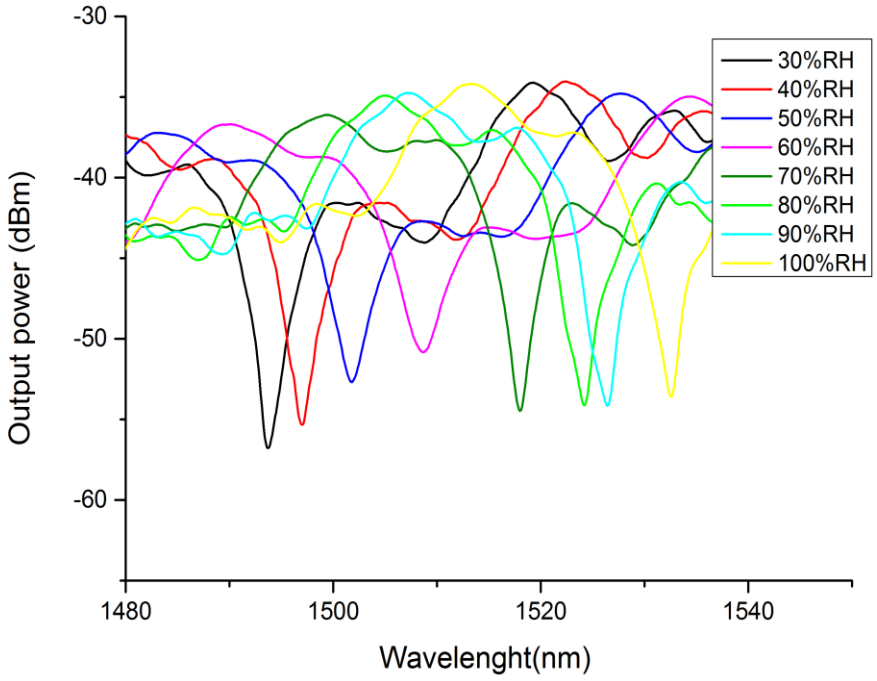

Figure (3.13): Transmission spectra of the SNCF sensor with relative humidity variation from 30% to 100% with diameters of 50µm coated with Al_2O_3- PVA thin films.

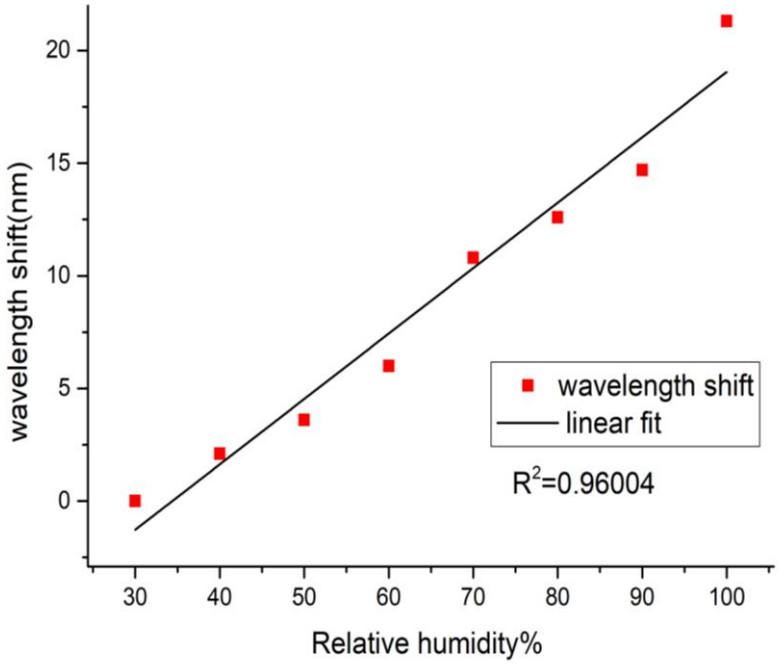

Figure (3.14): Response of the coated sensors to the variations of the relative humidity from 30% to 100% at 75 µm.

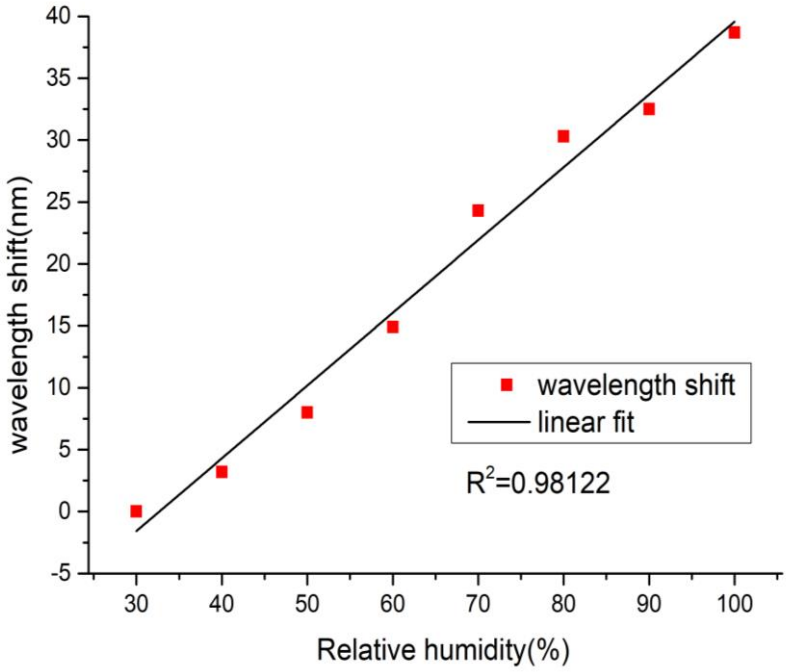

Figure (3.15): Response of the coated sensors to the variations of the relative humidity from 30% to 100% at 50 µm.

Table (3.1) summarizes the performance of 75, 50 µm coated sensors.

Table (3.1): Performance of the sensors decorated with Al_2O_3-PVA

Parameter	75 µm	50 µm
Sensitivity (nm/RH %)	0.295	0.587
Wavelength shift (nm)	21.3	38.9
Linearity (R^2) (%)	96.004	98.122

Finally, a parametric comparison with different relative humidity sensors is presented in Table (3.2). It clearly shows that the proposed sensor has a higher sensitivity than PVA alone, GQDs-PVA and CuO-PVA coatings and comparable performance to that of the GQDs-PVA hollow Core fiber sensor. As expect that the sensitivity could be enhanced further by reducing the waist diameter of NCF [92] and using an optimized concentration of the Al_2O_3-PVA composite.

Table (3.2): Performance comparison among various types of fiber-based RH sensors

Coating material	Structure	Sensitivity (nm/RH %)	RH Measurement range(%)	Ref.
PVA	SMS fiber	0.09	30-80	[78]
Au-PVA	D-shaped fiber	5.4	0-70	[83]
Agarose	SNCS fiber	0.149	30-75	[81]
LiCl	Multimode fiber (MMF)	0.164	20-95	[85]
GQDs-PVA	HCF	0.117	11.3-81.34	[87]
CuO-PVA	SNCS fiber	-0.581	30-100	[86]
PVA	U-shaped Microfiber	0.1865	30-95	[93]
Al_2O_3-PVA	SNCS fiber	0.587	30-100	Present work

To estimate one of the repeatability experiment features of the RH sensor figure (3.16) shows the sensor has a stable and linear response for the investigated RH with slight fluctuation, which possibly caused by temperature change and reading error of the optical spectrum analyzer (OSA). Also, the sensor has shown the same performance in different days of testing with different fabricated samples. Thus, the present sensor offers a good reproducibility. The response time of the seeded sensor was estimated by real-time observation from the OSA spectra when the RH of the chamber was increased from 30% to 100%. The measured response time was about 6s.

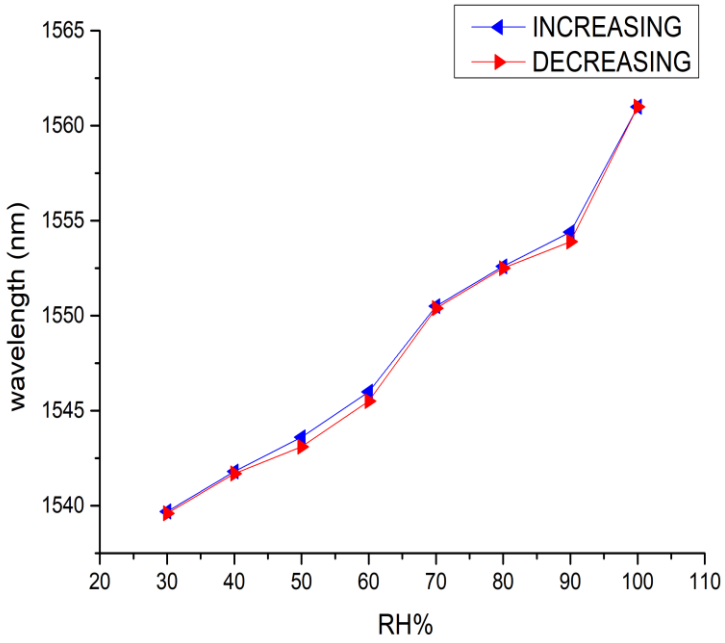

(a)

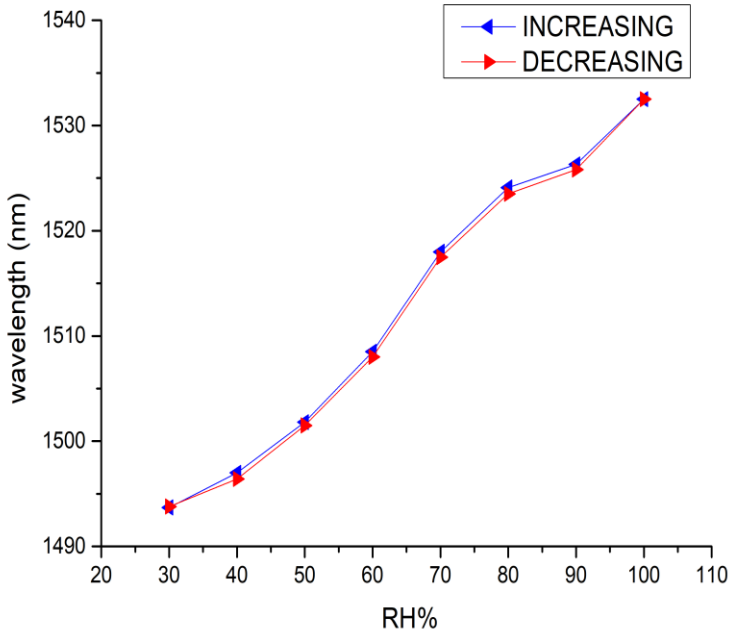

(b)

Figure (3.16): Wavelength repeatability of the coated sensors with variations of the relative humidity from 30% to 100% at diameter of: (a) 75 µm, (b) 50 µm.

3.6 The Rise Time of the OFHS based on SNCS fiber structure

To calculate the rise time of the proposed RH sensor, SNCS structure which coated with Al_2O_3-PVA (with specific length 20mm and diameter 50µm that shows the higher sensitivity to relative humidity variations) was exposed to an environment with rapid changes of the humidity. Firstly, keep the humidity inside the chamber at a low value 10% RH, and then rapidly increase the humidity of the chamber to a high value 100%.

Figure (3.17) shows the rise time measurement of the OFHS. The response time of the seeded sensor was estimated by real-time observation from the OSA spectra. The sensor has a fast response to RH variations and the measured response time was about (6 sec) when the RH changed from 30% to 100%

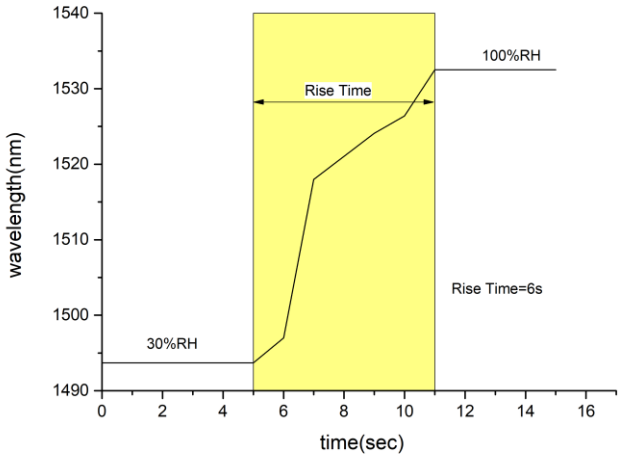

Figure (3.17): The rise time of the RH sensor with length (20mm) and 50µm diameter of NCF coated withAl_2O_3-PVA thin film.

3.7 Conclusion

An all-fiber optic for relative humidity detection based on multimode interference has been investigated and experimentally demonstrated. Fabrication

of SNCS structure involves only splicing short pieces of NCF (FG125LA from Thorlabs) between two standards SMF (Corning-28).

The conclusions obtained from this work are:

1. The sensor sensitivity of the RH depends on the NCF length, and the sensor with (20mm) NCF length is more sensitive to RH variations, in the RH ranges of (30-100%) are 0.265 nm/%RH, however for much longer NCF length (40, 60) mm the sensitivity decrease.
2. The obtained sensitivity has been improved when the diameter of the NCF etched from 125 μm to 50μm and obtained wavelength shift will increase toward the red shift.
3. A maximum obtained sensitivity at 0.262 nm/RH when the diameter of the NCF decreased to 50 μm with 20 mm length when the RH changes 30%RH to 100%RH.
4. The obtained wavelength shift will increase toward red shift when the RH increases 30%RH-100RH %.
5. RH sensor was improved by selected the optimum NCF length and diameter of sensor structure and coated with Al_2O_3-PVA thin film.
6. The maximum wavelength sensitivity of 0.587nm/%RH was attained for the RH range altering from 30% to 100%.
7. The sensor has a fast response to humidity variations, the rise time when the RH changes from 30%RH to 100%RH for this sensor with NCF length (20mm) and at wavelength (λ =1550nm) is equal (6sec).

3.8 Future Works

1. Decreasing the NCF diameter by chemical etching below 50 μm with length.
2. Recalculating the NCF length with the reduced diameter according to MMI theory to decrease the losses.
3. Can try different concentration of Al_2O_3 nanoparticles
4. Adding more layers of Al_2O_3-PVA.
5. Sensing enhancement of relative humidity sensor based on single mode fiber bend.

Reference

[1] I.R. Matias, F.J. Arregui, J.M. Corres, J. Bravo, “Evanescent Field Fiber-Optic Sensors for Humidity Monitoring Based on Nanocoatings”, IEEE Sensors Journal, 89–95 (2007).

[2] L. Alwis, T. Sun, K.T.V Grattan, “Optical Fibre-Based Sensor Technology for Humidity and Moisture Measurement: Review of Recent Progress, Measurement”, 46 4052–4074, (2013).

[3] S. Syafrani, A.M. Hatta, A. Kusumawardhani, “Relative Humidity Sensor Based on SMS Fiber Structure Using Multimode Coreless Fiber”, Proceedings of SPIE, in Second International Seminar on Photonics, Optics, and Its Applications (ISPhOA 2016), (2016).

[4] B. Du, D. Yang, X. She, Y. Yuan, D. Mao, Y. Jiang, F. Lu, “MoS2-Based All-Fiber Humidity Sensor for Monitoring Human Breath with Fast Response and Recovery”, Sensors and Actuators B: Chemical, 251 (2017).

[5] Q. Fei, Z. Qiang, K. Ni, Y. Yong, Y. Feng, Y. Ru, “Carbon-Nanotube / Polyvinyl Alcohol Coated Thin Core Fiber Sensor for Humidity Measurement”, Sensors and Actuators: B. Chemical, 800–806(2018).

[6] J. An, Y. Zhao, Y. Jin, C. Shen, “Relative Humidity Sensor based on SMS Fiber Structure with Polyvinyl Alcohol Coating”, Optik - International Journal for Light and Electron Optics, 124 (2013).

[7] W. Xu, J. Shi, X. Yang, D. Xu, F. Rong, J. Zhao, J. Yao, “Relative Humidity Sensor Based on No-Core Fiber Coated by Agarose-Gel Film”, Sensors, 17 2353(2018).

[8] Y. Chiu, C. Wu, C. Chiang, “Tilted Fiber Bragg Grating Sensor with Graphene”, Sensors, (2017).

[9] Y. Wang, C. Shen, W. Lou, F. Shentu, C. Zhong, X. Dong, L. Tong, "Fiber Optic Relative Humidity Sensor Based on the Tilted Fiber Bragg Grating Coated with Graphene Oxide", Applied Physics Letters,1-6031107,(2016).

[10] A. Alvarez-Herrero, H. Guerrero, D. Levy, "High-Sensitivity Sensor of Low Relative Humidity Based on Overlay on Side-Polished Fibers", In: Sensors, IEEE, Orlando, FL, USA, (2002).

[11] R. Gao, D. Lu, J. Cheng, Y. Jiang, L. Jiang, Z. Qi, "Humidity Sensor Based on Power Leakage at Resonance Wavelengths of a Hollow Core Fiber Coated with Reduced Graphene oxide", Sensors and Actuators B: Chemical, Vol(222),618–624,(2016).

[12] C. Teng, N. Jing, F. Yu, Y. Ding, J. Zheng, "Refractive Index Sensor Based on a Multi-Notched Plastic Optical Fiber", Applied Optics. 56 7–12, (2017).

[13] N. Jing, J. Zheng, X. Zhao, C. Teng, "Refractive Index Sensing Based on a Side-Polished Macrobending Plastic Optical Fiber", IEEE Sensors Journal, 15(5) 2898–2901, (2015).

[14] H. Dong, J. Guan, J. Yu, H. Lu, Y. Luo, J. Zhang, Z. Chen, Z. Wu, "Coreless Side Polished Fiber as Ultra-Sensitive Refractive Index Sensor", Proceedings of SPIE, 9899-98992S, (2016).

[15] D. Kim, J.U. Kang, "Sagnac Loop Interferometer Based on Polarization Maintaining Photonic Crystal Fiber with Reduced Temperature Sensitivity", Optics Express, 12 (19) 4490–4495, (2004).

[16] J.M. Corres, F.J. Arregui, I.R. Matias, "Design of Humidity Sensors Based on Tapered Optical Fibers, Journal of Lightwave Technology", 24(11) 4329–4336,(2006).

[17] M. Shao, X. Qiao, H. Fu, H. Li, J. Zhao, Y. Li, "A Mach–Zehnder Interferometric Humidity Sensor Based on Waist-Enlarged Tapers", Journal Optics and Lasers in Engineering, (52)86–90, (2014).

[18] L.D. Hart, E. Lense, Alumina Chemicals: Science and Technology Handbook, John Wiley and Sons, (1990).

[19] O. Apel, K. Mann, G. Marowsky, "Nonlinear Thickness Dependence of Two-Photon Absorptance in Al_2O_3 Films", Applied Physics A, (71) 593–596, (2000).

[20] T. Hadjifotiou, "The Cable and Telecommunications" ,(2009).

[21] E. A. AWAD "BASICS OF FIBER OPTICS" university of technology Iraq.

[22]H. Liu et al., "Relative Humidity Sensor Based on S-Taper Fiber Coated with SiO2 Nanoparticles," IEEE Sens. J., 15(6), 3424-3428, (2015).

[23] J. Cwalinski, P.E. " Introduction to Fiber Optics " Continuing Education and Development.

[24] laboratory of Laser Molecular Spectroscopy University of Lodz, Fundamentals of Optical Fiber Transmission, 1–49, (2011).

[25] K., Fidanboylu, and H.s.,Efendioglu, "Optical fiber Sensors and their Applications", 5 th International Advanced Technologies Symposium (IATS'09), Karabuk, Turkey, 13-15, May (2009).

[26] G.P. Agrawal, "Fiber-Optic Communication Systems", 3rd edition , Jhon Wiley & Sons Inc., ch2 23-36, (2002).

[27] S. M. Dhanshetti, "Advance Module Communication System and Specilized Module Dth And Other Communication System", India, (2015).

[28] https://www.thorlabs.com/newgrouppage9.cfm?objectgroup_id=7948 2017/09/06.

[29] W. A. Khaleel, A. Al-Janabi, "High-sensitivity sucrose erbium-doped fiber ring laser sensor", Opt. Eng. 56, 026116 (2017).

[30] P. V. Volkov, A. V. Goryunov, A. Y. Lukyanov, "Fiber optic temperature sensor based on low-coherence interferometry without scanning", Optik, Vol. 124, pp. 1982-1985, 2013.

[31] J. Estella, P. Vicente, J. Echeverria, J. Garrido, "A fibre optic humidity sensor based on a porous silica xerogel film as the sensing element", Sensors and Actuators B, Vol. 6, pp. 122-128, (2010).

[32] John M. Senior, "Optical Fiber Communications Principles and Practice", Third addition, England, (2009).

[33] L. Zou and O. M. Sezerman, "Method and system for simultaneous measurement of strain and temperature", United States Patent, US 7,599,047 B2, (2009).

[34] B.R. Mhdi, N.A. Aljbar, S. A. Kadhim, J.F. Hamode, A.H. Khalid, S.M. Ali, A.S. Mhdi, "Design Ammonia Gas Detection System by Using Optical Fiber Sensor", International Journal of Electronics Communication and Computer Engineering, 2278–4209, (2013)

[35] B.H. Timmer, K.M.v. Delft, R.P. Otjes, W. Olthuis, A.v.d. Berg, "A miniaturized measurement system for Ammonia in air", Anal. Chim. Acta 507 (1) 139–145, (2004).

[36] M. Born and E. Wolf, "Principles of Optics (7thed.)", Cambridge University Press, 1999.

[37] T.H. Xia, A. P. Zhang, B. Gu and J.J. Zhu, "Fiber optic refractive-index sensors based on transmissive and reflective thin-core fiber modal interferometers" ,Optics Communications, 283, 10 , (2010).

[38] W. C. Goss, R. Goldstein, M. D. Nelson, H. T. Fearnehaugh, and O. G. Ramer, "Fiber-optic rotation sensor technology", Applied Optics, 19,852-858 (1980).

[39] S. Qiu, Y. Chen, F. Xu, and Y. Lu, " Temperature sensor based on an isopropanol-sealed photonic crystal fiber in-line interferometer with enhanced refractive index sensitivity", Optics Letters, 37, 5, pp. 863-865,(2012).

[40] H. J. Patrick, G. M. Williams, A. D. Kersey, J. R. Pedrazzani, and A. M. Vengsarkar, "Hybrid fiber Bragg grating/long period fiber grating sensor for strain/temperature discrimination", IEEE Photonics Technology Letters. 8, 1223–1225 (1996).

[41] Minghong Yang, Jixiang Dai, Ciming Zhou, and Desheng Jiang, "Optical fiber magnetic field sensors with TbDyFe magnetostrictive thin films as sensing materials", Optics Express, 17, 23, 20777-20782 (2009).

[42] Wenhui Wang, Nan Wu, Ye Tian, Christopher Niezrecki, and Xingwei Wang, "Miniature all-silica optical fiber pressure sensor with an ultrathin uniform diaphragm", Optics Express, 18, 9, 9006-9014 (2010).

[43] Yi-Ping Wang, Limin Xiao, D. N. Wang, and Wei Jin "Highly sensitive long- period fiber-grating strain sensor with low temperature sensitivity", Optics Letters, 31, 23, 3414-3416 (2006).

[44] M. R. Layton and J. A. Bucaro, "Optical fiber acoustic sensor utilizing mode-mode interference", Applied Optics, 18, 5, 666-670 (1979).

[45] Lina Xu, Joseph C. Fanguy, Krunal Soni, and Shiquan Tao, “Optical fiber humidity sensor based on evanescent-wave scattering”, Optics Letters, 29, 11, 1191-1193 (2004).

[46] Shuichi Tai, Kazuo Kyuma, and Masahiro Nunoshita, “Fiber-optic acceleration sensor based on the photoelastic effect”, Applied Optics, 22,11, 1771-1774 (1983).

[47] M. E. Bosch, A. J. R. S´anchez, F. S. Rojas, and C. B. Ojeda, “ Recent development in optical fiber biosensors ”, Sensors journal, 7, 797–859, (2007).

[48] P. A. E. Piunno, U. J. Krull, R. H. E. Hudson, M. J. Damha, and H. Cohen, “Fiber optic biosensor for fluorimetric detection of DNA hybridization”, Analytica Chimica Acta, 288(3):205–214, (1994).

[49] S. C. Huang, W. W. Lin, M. T. Tsai, and M. H. Chen, “Fiber optic in-line distributed sensor detection and localization of the pipeline leaks”, Sensors and Actuators A, 135:570–579, (2007).

[50] A. Norouzi, A. H. Zaim, and B. B. Ustundag, "An integrated survey in Optical Networks: Concepts, Components and Problems", 11, 1, pp. 10-26, (2011).

[51] T. Kumagai, H. Soekawa, T. Yuhara, and H. Kajioka, “Fiber optic gyroscopes for vehicle navigation systems”, Proceedings of SPIE, 2070:181–191, (1994).

[52] A. M. R. Pinto and M. Lopez-Amo, “Photonic Crystal Fibers for Sensing Applications”, J. Sensors, Vol. 2012, pp. 1–21, (2012).

[53] B. Lee, “Review of the present status of optical fiber sensors”, Optical Fiber Technology, vol. 9, no. 2. pp. 57–79, (2003).

[54] M. Yusof, N. Khalili, and G. D. Peng, "All-Fiber Optic Humidity Sensor Based on Photonic Bandgap Fiber and Digital WMS Detection", IEEE Sensors Journal, vol. 13, no. 5, may (2013).

[55] X. Liu, J. Zheng, J. Yang, Y. Li, X. Dong, ''Refractive index sensor based on combination of tilted fiber Bragg grating and waist-enlarged fusion bitaper", Optics Communications 356 (2015) 571–573.

[56] C. Elosua, I. R. Matias, C. Bariain and F. J. Arregui, "Volatile Organic Compound Optical Fiber Sensors: A Review", *Sensors*, *6*(11), 1440-1465(2006).

[57] F. Zujie, C. Ken, Q. Ronghui, C. Haiwen, "Fundamentals of Optical Fiber Sensors", ISBN: 1118381734, John Wiley & Sons, (2012).

[58] S. Ghetia, R. Gajjar, P. Trivedi, "Classification of Fiber Optical Sensors", International Journal of Electronics Communication and Computer Technology, Vol.3, No.4, pp. 442-444, July 2013.

[59] S. Novais, M.S. Ferreira, L. Pinto, "Relative Humidity Fiber Sensor Based on Multimode Interferometer Coated with Agarose-Gel", Coatings, 8-453, (2018).

[60] D. Lopez-Torres, C. Elosua, J. Villatoro, J. Zubia, M. Rothhardt, K. Schuster, F.J, "Arregui, Enhancing Sensitivity of Photonic Crystal Fiber Interferometric Humidity Sensor by the Thickness of SnO_2 Thin Film", Sensors and Actuators B: Chemical, 251,1059–1067,(2017)

[61] A.B. Socorro, M. Hernaez, I.D. Villar, J.M. Corres, F.J. Arregui, I.R. Matias, "Single-Mode-Multimode-Single-Mode and Lossy Mode Resonance-Based Devices: A Comparative Study for Sensing Applications", Microsystem Technologies, 22(7)1633–1638, (2016).

[62] S. Choi, T. J. Eom, J. W. Yu, B. H. Lee, and K. Oh, "Novel All-Fiber Bandpass Filter Based on Hollow Optical Fiber", IEEE Photonics Technology Letters, 14, 12, pp. 1701-1703, (2002).

[63] L. Huang, G. Lin, M. Fu, H. Sheng, H. Sun and W. Liu, "A Refractive-index Fiber Sensor by Using No-Core Fibers", In Proceedings of the 2013 IEEE International Symposium on Next-generation Electronics, Kaohsiung, Taiwan, 25–26 February, pp. 100-102, (2013).

[64] J. Mathew, Y. Semenova and G. Farrell, "Photonic Crystal Fibre Interferometer for Humidity Sensing", Photonic Crystals - Introduction, Applications and Theory, (2012).

[65] J. Villatoro, V. Finazzi, G. Badenes and V. Pruneri, "Highly Sensitive Sensors Based on Photonic Crystal Fiber Modal Interferometers", Journal of Sensors, Spain, 1-11, (2009).

[66] A.J. Rodriguez-Rodriguez, D.A. May-Arrioja, I. Hernandez-Romano, I.R. Matias, "Multimode Interference Fiber Sensors for the Monitoring of Gasoline/Ethanol Blends, In: "I.R. Matias, et al. (eds.), Fiber Optic Sensors, Smart Sensors, Measurement and Instrumentation, 21", Springer International Publishing, Switzerland, 329-346, (2017).

[67] K. T. V. Grattau, B. T. Meggitt, "Optical Fiber Sensor Technology Advanced Applications - Bragg Gratings and Distributed Sensors", pp.1-3, (2000).

[68] J. Zhang, W. Chen, and C. Dong, "Fiber-optic sucrose sensor based on mode-filtered light detection", Journal of Carbohydrate Chemistry, 32, pp. 475-482, (2013).

[69] X. Jin, X. Huang, and L. Chen, "An Extrinsic Fabry–Perot Optical Fiber

Sensor Based on Nano-Magnetic Fluid", Fiber and Integrated Optics 32, pp. 233–24, (2013).

[70] Y. R. Garcia, J. Corres, and J. Goicoechea, "Vibration Detection Using Optical Fiber Sensors", Journal of Sensors, 2010, ID 936487, pp1-12,(2010).

[71] J.S. Krasiñski and G.W. Pearson, "Optical Nonreciprocal Devices and Their Applications", Proceedings of the International Conference "Quantum Optics III", Szczyrk, Poland, (1993).

[72] Z. Djinovi,M. Tomic, L. Manojlovic,Ž. Lazic, M. M. Smiljanic,"Non-contact Measurement of Thickness Uniformity of Chemically Etched Si Membranes by Fiber-Optic Low-Coherence Interferometry", Proc. 26th International Conference on Microelectronics (Miel 2008), Niš, Serbia , 11-14 May, (2008).

[73] J. Villatoro, V.P. Minkovich, V. Pruneri, G. Badenes, "Simple All-Microstructured-Optical-Fiber Interferometer Built Via Fusion Splicing", Optics Express. 15, 1491-1496, (2007).

[74] C. Zhao, X.Yang, C. Lu, W. Jin, and M. S. Demokan, "Temperature-insensitive interferometer using a highly birefringent photonic crystal fiber loop mirror", IEEE Photonics Technology Letters, 16, 11, pp. 2535–2537, (2004).

[75] Md. Faizul Huq ARIF, Kawsar AHMED, Sayed ASADUZZAMAN, and Md. Abul Kalam AZAD, "Design and Optimization of Photonic Crystal Fiber for Liquid Sensing Applications", PHOTONIC SENSORS, Vol. 6, No. 3, pp.279–288,(2016).

[76] Q. Wu,* Y. Semenova, J. Mathew, P. Wang, and G. Farrell, "Humidity sensor based on a single-mode hetero-core fiber structure", OPTICS LETTERS / Vol. 36, No.10, (2011).

[77] Yu Zhao, Yongxing Jin, Houhui Liang, Xinyong Dong Jianfeng Wang, "All-Fiber-Optic Sensor for Relative Humidity Measurement", International Conference on Electronics and Optoelectronics (ICEOE 2011).

[78] J. An, Y. Zhao, Y. Jin, C. Shen, "Relative humidity sensor based on SMS fiber structure with polyvinylalcohol coating," Optik , 124 , pp.6178– 6181, (2013).

[79] J. An, Y. Jin, M. Sun, and X.Dong, "Relative Humidity Sensor Based on SMS Fiber Structure With Two Waist-Enlarged Tapers", IEEE SENSORS JOURNAL, VOL. 14, NO. 8, AUGUST (2014).

[80] C. Huang, W. Xie, M. Yang, J. Dai, & B. Zhang, "Optical Fiber Fabry–Perot Humidity Sensor Based on Porous Al_2O_3 Film", IEEE Photonics Technology Letters, VOL. 27, NO. 20, Octobr (2015).

[81] W. Xu , J. Shi , X. Yang, , D.Xu, F. Rong, J. Zhao , J. Yao, " Relative humidity sensor based on No-Core fiber coated by Agarose-gel film," Sensors, 17, 2353(2017).

[82] D. L.Torres , et al., "Photonic crystal fiber interferometer coated with a PAH/PAA nanolayer as humidity sensor", 242, 1065-1072,April (2017).

[83] H.Yan, D. Han, M. Li, B. Lin, " Relative humidity sensor based on surface plasmon resonance of D-shaped fiber with polyvinyl alcohol embedding Au grating", Journal of Nanophotonics, (2017).

[84] Y. Zhao, Y.Peng, M.Chen, F.Xia, R.Tong, "U-shaped Microfiber Coupler Coated with Polyvinyl Alcohol Film for Highly Sensitive Humidity Detectio"", Sensors and Actuators A: Physical, (2018).

[85] Y.Zhao, Y.Yuan, W.Gan, M. Yang, “Optical fiber Fabry–Perot humidity sensor based on polyimide membrane: Sensitivity and adsorption kinetic”, Sensors and Actuators A: Physical, (2018).

[86] H. Alsweefe, S. K. Al-Hayali, A. Al-Janabi, “Efficient Humidity Sensor Based on an Etched No-Core Fiber Coated with Copper Oxide Nanoparticles”, Journal of Nanophotonics, 12(4) 046018(2018).

[87] Y.Zhao, R.Tong, M.Chen, F.Xia, “Relative humidity sensor based on hollow core fiber filled with GQDs-PVA”, Sensors and Actuators B: Chemical, (2019).

[88] Y. Liu, Y. Li, X. Yan, W. Li, “High Refractive Index Liquid Level Measurement via Coreless Multimode Fiber”, IEEE Photonics Technology Letters, 27(20) PP.2111-2114(2015).

[89] S. Azada, E. Sadeghia, R. Parvizia, A. Mazaheri, M. Yousefi, “Sensitivity optimization of ZnO clad-modified optical fiber humidity sensor by means of tuning the optical fiber waist diameter”, Opt. Laser Technol. 90, 96-101(2017).

[90] W. Yao, X. Chen, J. Zhang, “A Capacitive Humidity Sensor Based on Gold–PVA Core–Shell Nanocomposites”, Sensors and Actuators, B: Chemical, 145 PP. 327-333, (2010).

[91] C. li, R. Fu, C. Yu, Z. Li, H. Guan, D. Hu, D. Zhao, L. Lu, “Silver Nanoparticle/Chitosan Oligosaccharide/Poly(vinyl alcohol) Nanofibers as Wound Dressings A Preclinical Study”, International Journal of Nanomedicine, 8,PP. 4131–4145,(2013).

[92] Y. Peng, Y. Zhao,M. Q. Chen, and F. Xia, “Research Advances in Microfiber Humidity Sensors”, Small, 14:1800524,PP.1-20,(2018).

[93] Y. Zhao, Y. Peng, M. Q. Chen, R. J. Tong, "Humidity Sensor Based on Unsymmetrical U-shaped Microfiber with a Polyvinyl Alcohol Overlay", Sensors and Actuators B,PP.312-318,(2018).

[94] K. A. Fidanboylu, and H. S. Efendioglu, "Fiber Optic Sensors and Their Applications", International Advanced Technologies Symposium (IATS'09), Vol. 6 , pp.1-6 , May 2009.

[95] S.A.Mohammed, and A. H.Al-Janabi , "All Fiber Chemical Liquids Refractive Index Sensor Based on Multimode Interference" Iraqi J. Laser, Vol.17,pp.33-39,(2018).

[96] S.S. Hindal, and H. J. Taher, "Performance of humidity sensor based on photonic crystal fiber interferometer" Iraqi Journal of Physics, Vol.14 , No.30, PP. 83-89 ,(2016).

Appendix
(A)

Superluminescent Diode
1550 nm, Butterfly Package

SLD1550S-A1

Description

The SLD1550S-A1 is a 1550 nm, low-power, broadband Superluminescent Diode (SLD) with a near-Gaussian spectral profile and low ripple. This SLD is housed in a standard 14-pin butterfly package with FC/APC-connectorized, nonpolarization-maintaining fiber. An integrated thermistor allows for temperature control, thus stabilizing the power and spectrum.

Specifications

CW; T_{CHIP} = 25° C, T_{CASE} = 0 to 65° C

SLD1550S-A1				
	Symbol	Min	Typical	Max
Center Wavelength	λ_C	1520 nm	1550 nm	1580 nm
Operating Current	I_{OP}	-	450 mA	500 mA
ASE Power*	P_{ASE}	0.75 mW	1.0 mW	-
Optical 3 dB Bandwidth*	BW	100 nm	110 nm	-
RMS Gain Ripple *	ΔG	-	-	0.1 dB
Forward Voltage*	V_F	-	1.6 V	2.0 V
TEC Operation (Typical / Max @ T_{CASE} = 25 °C / 65 °C)				
- TEC Current	I_{TEC}	-	0.35 A	1.5 A
- TEC Voltage	V_{TEC}	-	0.5 V	3.5 V
- Thermistor Resistance	R_{TH}	-	10 kΩ	-

*@I_{OP}

Performance Plots

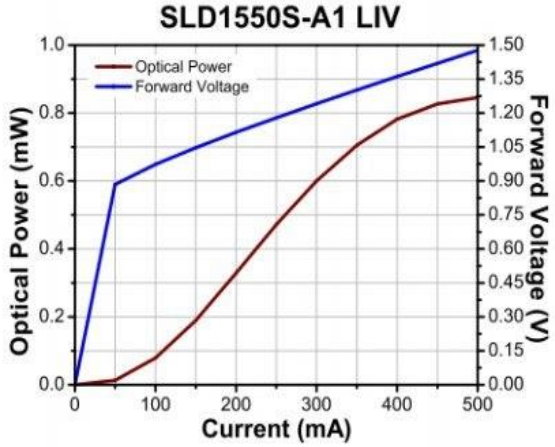

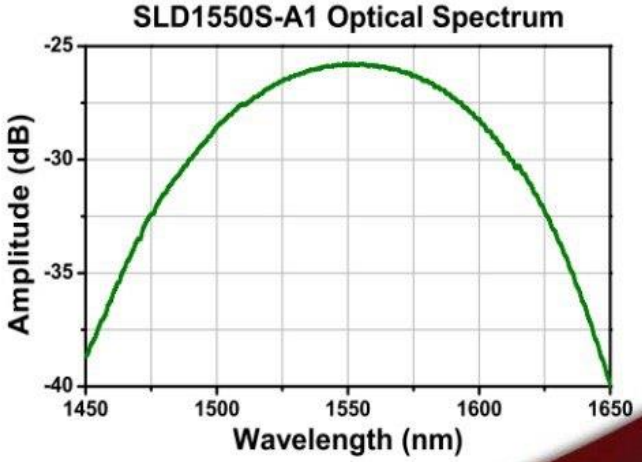

Drawings

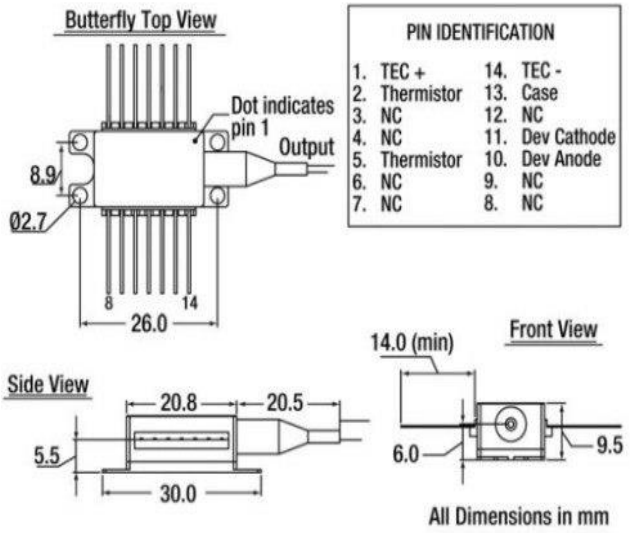

PIN IDENTIFICATION			
1.	TEC +	14.	TEC -
2.	Thermistor	13.	Case
3.	NC	12.	NC
4.	NC	11.	Dev Cathode
5.	Thermistor	10.	Dev Anode
6.	NC	9.	NC
7.	NC	8.	NC

All Dimensions in mm

Note: Output isolator and monitor photodiode are available options for butterfly-packaged diodes. Please contact Technical Support for more information.

Appendix
(B)

Corning® SMF-28® Ultra Optical Fiber

Product Information

CORNING

Corning® SMF-28® Ultra optical fiber is an ITU-T Recommendation G.652.D compliant optical fiber with Corning's enhanced low-loss and bend fiber technologies. This full-spectrum fiber has bend performance that exceeds the ITU-T Recommendation G.657.A1 standard and still splices the same as the installed base of standard single-mode fibers such as SMF-28e+ fiber. SMF-28 Ultra fiber offers industry-leading specifications for attenuation, macrobend loss, and polarization mode dispersion values, which provide a solid foundation for new network deployments as well as upgrades to existing networks. Since Corning brought the first fiber to market more than 40 years ago, Corning's leadership in single-mode fiber innovation has been unparalleled.

Optical Specifications

Maximum Attenuation

Wavelength (nm)	Maximum Value* (dB/km)
1310	≤0.32
1383**	≤0.32
1490	≤0.21
1550	≤0.18
1625	≤0.20

* Alternate attenuation offerings available upon request.
** Attenuation values at this wavelength represent post-hydrogen aging performance.

Attenuation vs. Wavelength

Range (nm)	Ref. λ (nm)	Max. α Difference (dB/km)
1285–1330	1310	0.03
1525–1575	1550	0.02

The attenuation in a given wavelength range does not exceed the attenuation of the reference wavelength (λ) by more than the value α.

Macrobend Loss

Mandrel Radius (mm)	Number of Turns	Wavelength (nm)	Induced Attenuation* (dB)
10	1	1550	≤0.50
10	1	1625	≤1.5
15	10	1550	≤0.05
15	10	1625	≤0.30
25	100	1310, 1550, 1625	≤0.01

*The induced attenuation due to fiber wrapped around a mandrel of a specified radius.

Point Discontinuity

Wavelength (nm)	Point Discontinuity (dB)
1310	≤0.05
1550	≤0.05

Cable Cutoff Wavelength (λ_{cc})

$\lambda_{cc} \leq 1260$ nm

Mode-Field Diameter

Wavelength (nm)	MFD (μm)
1310	9.2 ± 0.4
1550	10.4 ± 0.5

Dispersion

Wavelength (nm)	Dispersion Value [ps/(nm.km)]
1550	≤18.0
1625	≤22.0

Zero Dispersion Wavelength (λ_0): 1304 nm ≤ λ_0 ≤ 1324 nm
Zero Dispersion Slope (S_0): $S_0 \leq 0.092$ ps/(nm² · km)

Polarization Mode Dispersion (PMD)

	Value (ps/√km)
PMD Link Design Value	≤0.04*
Maximum Individual Fiber PMD	≤0.1

*Complies with IEC 60794-3: 2001, Section 5.5, Method 1, (m = 20, Q = 0.01%), September 2001.

The PMD link design value is a term used to describe the PMD of concatenated lengths of fiber (also known as PMD_Q). This value represents a statistical upper limit for total link PMD. Individual PMD values may change when fiber is cabled.

How to Order

Contact your sales representative, or call the Optical Fiber Customer Service Department:
Ph: 1-607-248-2000 (U.S. and Canada)
+44-1244-525-320 (Europe)
Email: cofic@corning.com
Please specify the fiber type, attenuation, and quantity when ordering.

Dimensional Specifications

Glass Geometry

Fiber Curl	≥ 4.0 m radius of curvature
Cladding Diameter	125.0 ± 0.7 µm
Core-Clad Concentricity	≤ 0.5 µm
Cladding Non-Circularity	≤ 0.7%

Coating Geometry

Coating Diameter	242 ± 5 µm
Coating-Cladding Concentricity	< 12 µm

Environmental Specifications

Environmental Test	Test Condition	Induced Attenuation 1310 nm, 1550 nm, and 1625 nm (dB/km)
Temperature Dependence	−60°C to +85°C*	≤ 0.05
Temperature Humidity Cycling	−10°C to +85°C up to 98% RH	≤ 0.05
Water Immersion	23°C ± 2°C	≤ 0.05
Heat Aging	85°C ± 2°C	≤ 0.05
Damp Heat	85°C at 85% RH	≤ 0.05

*Reference temperature = +23ºC

Operating Temperature Range: -60ºC to +85ºC

Mechanical Specifications

Proof Test

The entire fiber length is subjected to a tensile stress ≥ 100 kpsi (0.69 GPa).*

*Higher proof test levels available.

Length

Fiber lengths available up to 63.0 km/spool.

Performance Characterizations

Characterized parameters are typical values.

Core Diameter	8.2 µm
Numerical Aperture	0.14 NA is measured at the one percent power level of a one-dimensional far-field scan at 1310 nm.
Effective Group Index of Refraction (N_{eff})	1310 nm: 1.4676 1550 nm: 1.4682
Fatigue Resistance Parameter (N_d)	20
Coating Strip Force	Dry: 0.6 lbs. (3N) Wet, 14-day room temperature: 0.6 lbs. (3N)
Rayleigh Backscatter Coefficient (for 1 ns Pulse Width)	1310 nm: −77 dB 1550 nm: −82 dB

CORNING

Corning Incorporated
One Riverfront Plaza
Corning, NY 14831 U.S.A.
Ph: 607-248-2000 (U.S. and Canada)
+44-1244-525-320 (Europe)
Email: cofic@corning.com
www.corning.com/opticalfiber

Appendix
(C)

THORLABS

Coreless Termination Fiber

FG125LA
FG250LA
FG400LA

Description

These coreless silica termination fibers can be spliced to the ends of standard fiber to reduce back reflections or prevent damage to the fiber end face. A return loss of greater than 65 dB is achieved by splicing 0.25 m of coreless fiber to the desired component.

Specifications

Specifications			
Item #	FG125LA	FG250LA	FG400LA
Wavelength Range	400 - 2400 nm		
Return Loss	>65 dB with 0.25 m		
Glass Diameter	125 ± 1 µm	250 ± 10 µm	400 ± 15 µm
Coating Diameter	250 µm ± 5%	400 ± 20 µm	550 ± 20 µm
Coating	Acrylate		
Glass Refractive Index	1.467287 @ 436 nm 1.458965 @ 589.3 nm 1.450703 @1020 nm 1.444 @1550 nm		
Operating Temperature	-40 to 85 °C		
Proof Test Level	>100 kpsi		
Recommended Stripping Tool	T06S13 or FTS4	T12S16	T18S25

Appendix
(D)

Al_2O_3 Nanopowder Specification Sheet

Specification

Aluminium Oxide
(Al_2O_3, 99.9%, APS: 20nm)
Stock No. NS6130-03-303, CAS: 1344-

Product	:	**Aluminium Oxide**
Stock No	:	NS6130-03-
CAS	:	1344-28-
Particle	:	20 nm
Purity	:	99. %
Molecular	:	Al_2O_3
Molecular	:	101.9 g/mol
Density	:	3.95- g/cm³
Melting	:	207 °C
Boiling	:	297 °C
PH Value	:	6.
SSA	:	15- m^2/g
Color	:	White
Crystal	:	Neutral
Main Inspect	:	**Manager**
Date of	:	**August 10.**
Version	:	**1**

NoteProduct Specification are subject to amendment may change over time

Intelligent Materials Pvt. Ltd.
www.nanoshel.com, sales@nanoshel.com

NANOSHEL
Creating Miracles in Black

Characterization of Aluminium Oxide Nanopowder

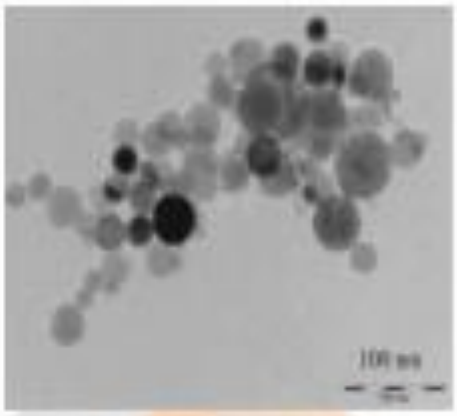

SEM of Aluminium Oxide Nanopowder

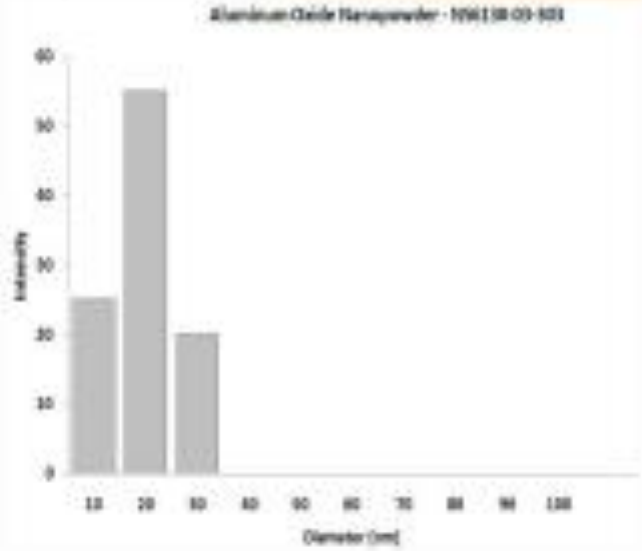

Particle Size Analysis of Aluminium Oxide Nanopowde

NANOSHEL LLC
3422 Old Capitol Trial Suit 1305, Wilmington DE - 19808 USA
(001) 302-652-3464, + 91 9779-680077

الخلاصة

تستخدم متحسسات الرطوبة للألياف البصرية (RH) القائمة على التداخل متعدد الانماط (MMI) لليف خالي القلب المحفور كيميائيا على نطاق واسع في مجال الاستشعار. تم بناء المستشعر عن طريق تركيب ليف ضوئي خالي القلب (NCF) بين نوعين من الألياف أحادية الطور (SMF). لتحسس التغير بالرطوبة المحيطة ، تم الحصول على اقطار مختلفة من الليف خالي القلب (NCF) (125 و 100 و 75 و 50)ميكرومتر، مع طول ثابت قدره 20 ملم من الليف خالي القلب (NCF) بعملية الحفر الكيميائي بواسطة حامض الهيدروفلوريك (HF). ايضا تم بناء المتحسس بواسطة لحام الاطوال (60 ، 40 ، 20) ملم من الليف خالي القلب(NCF) مع القطر الأمثل 50 مايكرومتر بين نوعين من الألياف أحادية الطور (SMF) لدراسة تأثير الطول على حساسية المستشعر. الأداء الأمثل لجهاز الاستشعار المقترح في استشعار التباين في الرطوبة النسبية كان لليف خالي القلب بقطر 50 ميكرومتر وطول 20 ملم لهيكل الاستشعار ، وتكشف النتائج التجريبية انه تم الحصول على ما يقرب اكثر من ضعفين زيادة في الحساسية للقطر الامثل المغلف مع جزيئات أكسيد الألمنيوم النانوية (Al_2O_3 NPs) المضمنة في بولي فينيل الكحول (PVA). تم الحصول على اعلى حساسية قدرها 0.587 نانومتر /الرطوبة النسبية على التوالي في نطاق رطوبة 30 ٪ إلى 100 ٪ وكانت سرعة الأستجابة مع الزمن مع زمن استجابة ٦ ثانية. يمكن لجهاز الاستشعار المقترح إنشاء مصدر واعد لمراقبة التغير بالرطوبة النسبية.

وزارة التعليم العالي والبحث العلمي
جامعة بغداد
معهد الليزر للدراسات العليا

تحسين متحسس الرطوبة النسبية المعتمد في بناءه على التداخل المتعدد الانماط للالياف منزوعة القلب باستخدام جسيمات أكسيد الالمنيوم النانوية المضمنة في بولي فينيل الكحول

رسالة مقدمة الى

معهد الليزر للدراسات العليا /جامعة بغداد /لاستكمال متطلبات نيل شهادة ماجستير علوم في الليزر/ هندسة الكترونيك واتصالات

من قبل

هبه ياسين ذيبان

بكالوريوس هندسة الليزر والالكترونيات البصرية - ٢٠١٥

بإشراف

د. حنان جعفر طاهر

١٤٤١ هـ **٢٠٢٠ م**